3D SCANNER IMPLEMENTATION FOR SHINY SURFACES USING COLOR INVARIANTS

by

Rıfat Benveniste

Submitted to the Institute of Graduate Studies in
Science and Engineering in partial fulfillment of
the requirements for the degree of
Master of Science
in
Electrical and Electronics Engineering

Yeditepe University

2007

3D SCANNER IMPLEMENTATION FOR SHINY SURFACES USING COLOR INVARIANTS

APPROVED BY:

Assist. Prof. Dr. Cem Ünsalan . . . . . .
(Thesis Supervisor)

Assoc. Prof. Dr. Canbolat Uçak . . . . . .

Assist. Prof. Dr. Ender Özcan . . . . . .

DATE OF APPROVAL: .....

ACKNOWLEDGEMENTS

I would like to thank to the valuable people who supported me during this long and hard project.

I especially thank to my supervisor Assist. Prof. Dr. Cem Ünsalan for his motivating comments, corrections and guiding me with useful suggestions during the thesis.

I am most grateful to my family for providing me great opportunities to improve myself and for their continuous support in my life.

I also want to express my appreciation for my girlfriend Duygu Birecikli who is certainly the main contributor of all the best in my life. I would like to thank for her everlasting patience and support as a friend and a companion.

I would also like to thank to all my professors in Electrical and Electronics Engineering Department for teaching me the necessary knowledge during my undergraduate and graduate educations.

ABSTRACT

3D SCANNER IMPLEMENTATION FOR SHINY SURFACES USING COLOR INVARIANTS

The improvements on computer systems derived the need of digitizing the objects of the real world. The game and movie industry needs 3D models of objects for computer graphics applications. Also, 3D modelling is widely used in the areas of rapid prototyping, medical applications and cultural heritage protection facilities. There are various types of scanners designed according to these application areas. We can summarize the types of 3D scanners under two main headings. The scanners with surface contact and without contact. The surface touch scanners are the type of the scanners that contact to the surface. They are used in many applications but they are not applicable for the objects with hard to reach parts. The time of flight scanners and triangulation based structured light scanners are the types of non contact scanners. The time of flight scanners work on principle of measuring the time of photon to fly to the object. This gives a high resolution result but it is a slow system. The structured light scanners are based on triangulation principle. A special pattern or a stripe is projected to the object. The stripe deforms according to the 3D structure of the surface. This deformation of the stripe is captured by a camera placed with a known angle to the object. This orientation creates a triangular shape. By simple trigonometric calculations based on this triangle, the depth information is extracted.

The extraction of stripe information from the captured image is made by image processing. The surface structure of the object and the lighting conditions of the medium affects the quality of the captured image. The illumination of the medium creates glowing parts and highlights on the shiny or specular surfaces. This can be considered as noise on the image processed. Some filtering applications are used to solve this problem, but they do not overcome the problem entirely. In practice, powder like opaque materials are used to cover such surfaces to reduce the specularity of the surface. However, objects like archeological

findings need special treatment. Therefore, applying powder may result with damages on the surface of the object.

This study focuses on solving the problem of scanning shiny surfaces in an illuminated medium. We propose using the color invariants to solve this problem. Color invariants help extracting color properties of objects without being affected by imaging conditions like the illumination of the environment and the surface properties of the object. We propose a new invariant and implement it with two types of scanners. We designed and implemented a laser scanner and a stripe projecting scanner. We performed experiments on shiny and matte surfaced objects and observed the success of the invariant implemented on the system. We also tested the invariants proposed in literature and compared the results on given conditions. The results of the experiments showed that the color invariant we proposed can extract the line information both on shiny and matte surfaces successfully. The other invariants proposed in literature also had success on different surfaces and some did not. As a result of whole system setup, we obtained 3D models of the objects with shiny surfaces and matte surfaces successfully.

ÖZET

RENK DEĞİŞMEZLERİ KULLANARAK PARLAK YÜZEYLER İÇİN ÜÇ BOYUTLU TARAYICI GERÇEKLENMESİ

Bilgisayar sistemlerindeki gelişmeler, gerçek dünyadaki nesneleri sayısallaştırma ihtiyacını beraberinde getirdi. Bilgisayar grafiği uygulamaları için, oyun ve film endüstrisi, nesnelerin üç boyutlu modellerine ihtiyaç duymaktadır. Üç boyutlu modelleme, hızlı prototip üretme, tıbbi uygulamalar ve kültürel mirası koruma alanlarında da geniş ölçüde kullanılmaktadır. Bu uygulama alanlarına yönelik değişik tarayıcı türleri tasarlanmıştır. Üç boyutlu tarayıcı türlerini iki ana başlık altında özetleyebiliriz: Yüzey teması olan tarayıcılar ve yüzey teması olmayan tarayıcılar. Yüzeye dokunan tarayıcılar, yüzey teması olan tarayıcılar türündendir. Pek çok uygulamada kullanılırlar, ancak ulaşılması zor kısımları olan nesneler için uygulanamazlar. Time of flight tarayıcılar ve üçgenleme tabanlı structured light tarayıcılar yüzey teması olmayan tarayıcıların türleridir. Time of flight tarayıcılar fotonun nesneye ulaşma zamanını ölçme prensibi ile çalışırlar. Bu tür tarayıcılar, yüksek çözünürlüklü sonuç verir, ama yavaş sistemlerdir. Structured light tarayıcılar, üçgenleme prensibine dayanır. Nesneye özel bir desen veya bir şerit yansıtılır. Yüzeyin üç boyutlu yapısına göre, şerit deformasyona uğrar. Şeridin bu deformasyonu, nesneye bilinen bir açı ile bakan kamera tarafından yakalanır. Bu yerleştirme, üçgen şeklini oluşturur. Bu üçgeni temel alan basit trigonometrik hesaplar ile, derinlik bilgisi elde edilir.

Çekilen görüntü üzerindeki çizgi bilgisini elde etmek için imge işleme kullanılır. Nesnenin yüzey yapısı ve ortamın ışıklandırma koşulları, yakalanan görüntünün kalitesini etkiler. Parlak veya yansıyan yüzeylerde, ortamın aydınlatması parlayan yüzeyde ışığın görüldüğü kısımlar yaratır. Bu kısımlar, işlenen görüntü üzerinde gürültü olarak görünür. Bu problemi çözmek için birtakım filtreleme uygulamaları kullanılır, ancak bunlar problemi tamamen çözmezler. Pratikte, yüzeyin yansımasını azaltmak için, yüzey pudra gibi yansıtıcılığı olmayan maddeler ile kaplanır. Ancak, arkeolojik bulgularda elde edilen nesnelerde yüzeye

özen göstermek gerekir. Bu nedenle, bu tür nesnelerde pudra uygulamak nesnenin yüzeyine zarar verebilir.

Bu çalışma, parlak yüzeyleri aydınlık ortamda tarama probleminin çözümü üzerinde odaklanmıştır. Biz, bu problemi çözmek için renk değişmezlerini kullanmayı öneriyoruz. Renk değişmezleri, çekilen görüntüde şeridin rengini vurgular. Bu yüzden şerit çıkarımı, aydınlatma şartlarından ve nesnenin yüzey yapılarından etkilenmez. Yeni bir değişmez öneriyoruz ve bunu iki tür tarayıcıda gerçekleştirdik. Bir lazer tarayıcı ve bir şerit yansıtan tarayıcı tasarladık ve gerçekleştirdik. Parlak ve mat yüzeyli nesneler üzerinde deneyler yaptık ve sistem üzerinde gerçekleştirdiğimiz değişmezin başarısını gözlemledik. Literatürde önerilen değişmezleri denedik ve verilen şartlarda elde edilen sonuçları karşılaştırdık. Deneylerin sonuçları gösterdi ki, önerdiğimiz renk değişmezi hem parlak hem de mat yüzeylerde çizgi bilgisini başarıyla çıkarabiliyor. Literatürde önerilen diğer değişmezlerden bazıları farklı yüzeylerde başarılıydı. Sonuç olarak kurulan sistemde, parlak yüzeyi olan ve olmayan nesnelerin üç boyutlu modellerini başarıyla elde ettik.

TABLE OF CONTENTS

LIST OF FIGURES

LIST OF SYMBOLS/ABBREVIATIONS

f_l	Focal length of camera
θ	Angle of the camera
3D	Three Dimensional
A	Ampere
CCD	Charge Coupled Device
cm	Centimeter
FIR	Finite Impulse Response
IEEE	Institute of Electrical and Electronics Engineers
LCD	Liquid Crystal Digital
m	Meter
mm	Millimeter
nm	Nanometer
PAL	Phase Alternating Line
PCA	Principal Component Analysis
RGB	Red Green Blue
$R(\lambda)$	Sensor Response
TTL	Transistor Transistor Logic
V	Volt

1. INTRODUCTION

Digitalized three dimensional representation of actual physical objects are used in various applications. Therefore, there is a strong need for devices to transfer the depth information of a physical object to the computer environment. 3D scanners are devices used to extract the surface coordinates of physical objects. There are different kinds of 3D scanners for use in different application areas. In the following sections we will give a brief explanation on different scanner types and their application areas. We also define the main problem considered in this study. We briefly explain the implementation of the proposed solution both in software and hardware.

1.1. Application Areas of 3D scanners

3D scanners are used in various areas such as reverse engineering, computer graphics, cultural heritage or archeological finding scanning, and medical imaging. Some application examples can be seen in Fig. 1.1. They are basically for, reverse engineering, animation movie, medical application, and cultural heritage.

In reverse engineering, 3D scanners are used for modeling and recovering broken or decayed piece of an industrial machinery. In movie industry, the character sculptures or objects placed in 3D animation movies are scanned and processed in computer graphics softwares. In the medical applications, doctors use the scan data in their orthopedical and reconstruction surgery preparations. In the dental applications, the jaw structure of patient is scanned to construct an appropriate teeth model. In cultural heritage preservation, these scanners are used for reconstruction or archiving the objects in digital databases like virtual museums.

1.2. Types of 3D scanners

There are various methods used to construct 3D scanners. Two main categories of 3D scanners are non-contact and contact. 3D scanners based on the touch sensors can be

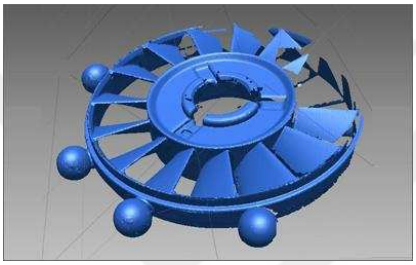

(a) Industry

(b) Animation movie

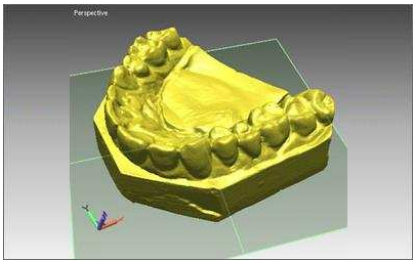

(c) Dental modeling

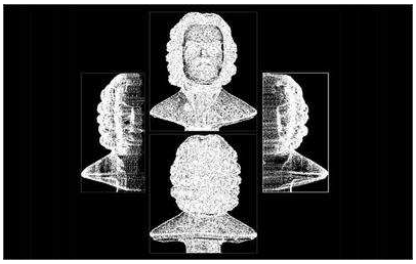

(d) Cultural heritage

Figure 1.1. Various application areas of 3D scanners

counted as of contact type. These devices are slow and do not have general usability. One main reason is that, touching might not be possible for some objects, either due to the object properties or their position. Non-contact scanners can also be divided into two basic categories: triangulation based structured light and other optical property based. Triangulation based structured light non-contact scanners are based on different methods such as: line laser based, projection line based, and patterned structured light based. Patterned structured light based scanners use different pattern codification strategies such as coding by color and line width. In Fig. 1.2, we provide working examples for these scanners. Next, we will briefly explain the working principles of these scanners.

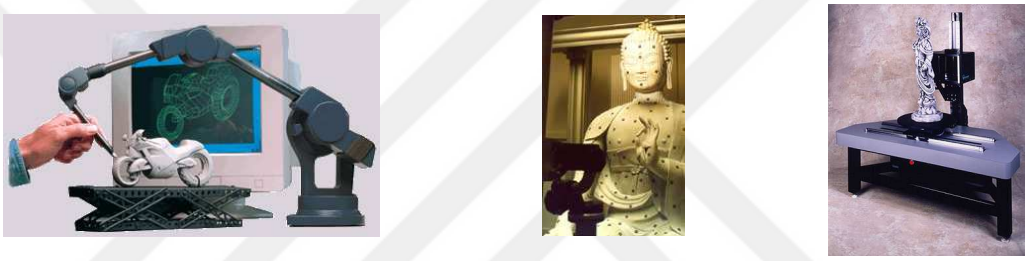

(a) Surface touch scanner (b) Time of flight scanner (c) Structured light scanner

Figure 1.2. Examples of different types of 3D scanners

1.2.1. Surface Touch Scanners

These are the earliest designed systems for 3D scanning. They are extensively used in automotive industry. Fig. 1.2 (a) shows an example of this type of scanner used to scan clay model of a motorcycle. The working principle of the surface touch scanner is as follows. A special pen type sensor is touched and moved over the whole object surface. The system senses changes in depth and transfers this information to a computer as a three dimensional point cloud. This type of scanner may have serious problems while scanning objects with hard to reach parts.

1.2.2. Time of Flight Scanners

This type of scanner work on the principle of measuring the time of the photon flying to and from the object. A point light source (mostly a point laser) is used for this purpose.

The light source projects the point on an object surface. An optic sensor measures the hit and return time of the point light. By calculating the duration of light on each point on the object, the depth information is acquired. Since the object is scanned point by point, these scanners are very slow. They are mostly used in applications that require very high resolution. Since these scanners, on a point basis, they can provide this resolution easily.

1.2.3. Structured Light Scanners

The basic working principle of triangulation based structured light 3D scanners can be described as follows. A monochromatic or multispectral laser line, or a colored light stripe is projected from a light source on to the physical object. The projected light is then reflected back. One or more cameras acquire images of this reflection. The light pattern is detected from the acquired image. Then, the shape information is derived from triangulation. As the stripe is moved along the object surface, the 3D depth information of the physical object is obtained. Structured light scanners can further be divided into two main categories as line laser and pattern projecting scanners. In Fig. 1.3, we provide these two scanners. Next, we briefly explain them.

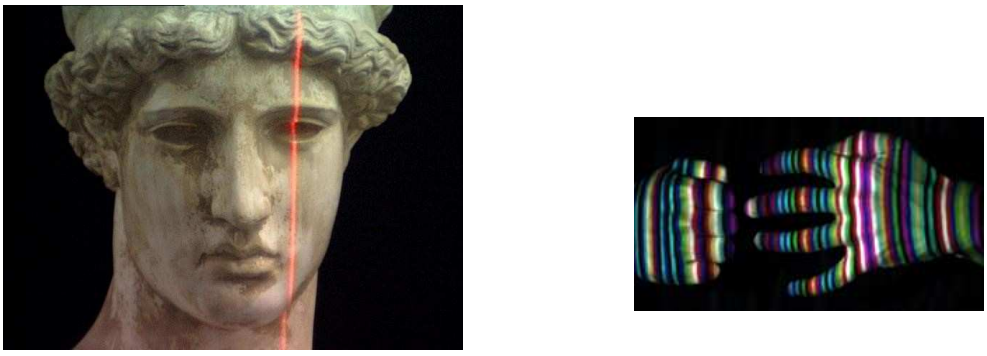

(a) Line laser (b) Pattern projection

Figure 1.3. Examples for structured light 3D scanners

1.2.3.1. Line Laser Scanners. This type of scanner projects a laser line stripe to the object. This is shown in Fig. 1.3 (a). Then, the image of the reflected light stripe is captured. As can be seen in the figure, the laser stripe is deformed according to the 3D shape of the object surface. The deformation of the stripe on the object gives the depth data with a simple

trigonometric calculation (called as triangulation). The width of the laser line affects the resolution of the scanned data. As the laser gets thinner, the deformation on the surface increases. Therefore, the object surface can be scanned in detailed form. Also, the movement of the line stripe on the object is important to have an accurate depth information.

1.2.3.2. Pattern Projecting Scanners. In patterned structured light scanners, there is more than one line projected on the object at the same time. Therefore, there is a well-known stripe matching problem in these scanner systems. To solve this problem, different codification strategies are applied to the projected pattern. The color coded pattern given in Fig. 1.3 (b) is a good example for codification.

1.3. Scanning Shiny Surfaces

A problem with structured light 3D scanning is that, the properties of the surface and the lighting conditions of the medium affect the quality of the image acquired. As a result, under some conditions the scanner can not be used. One such problem occurs while scanning physical objects with shiny or specular surfaces. Projected structured light stripes create glare on the object surface due to its specularity.

Some filtering techniques are proposed to solve this problem, but they do not work effectively. In practice, most of the shiny surfaced objects are covered with opaque materials such as powder to suppress the specularity on the surface. There are two major problems with this solution. First, covering all of the materials with powders slow down the scanning process. Second, some objects can not be covered with powder due to their properties.

The objective of this study is to find a solution to scan objects with shiny surfaces under daylight. We propose to use color invariants in a structured light scanning system. Color invariants emphasize the color of the stripe in the acquired image. Hence, the stripe extraction is not affected by external illumination factors. We introduce a new color invariant for use in this study. We also test existing color invariants proposed in the literature to solve our problem.

We develop two structured light scanners both in hardware and software to scan real shiny objects. The first scanner is based on line laser and the second scanner is based on a projection system. In the following chapters, we discuss their properties in depth.

Fig. 1.4 shows a block diagram of the triangulation based scanner system. In this system, there is a light source projecting light stripe onto the object. The object is placed on a rotating table to be scanned from different angles. The camera is located near to the light source with a known angle. This orientation of the camera and the light source forms a triangle. By simple trigonometric calculations based on this triangle, the depth information is extracted. To control the position of the light source and process the image captured, we use a personal computer. The software environment for this system is Matlab.

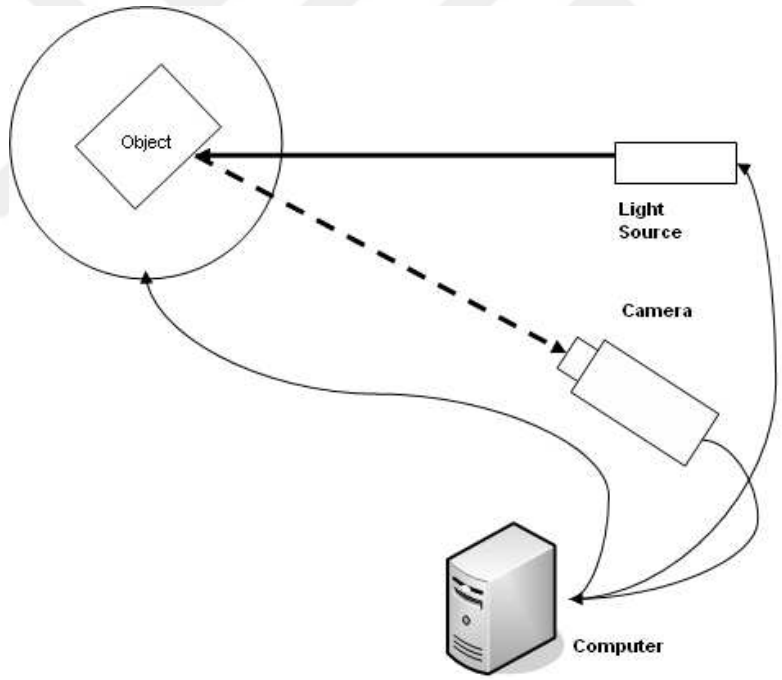

Figure 1.4. Block diagram of the triangulation based scanner.

2. PREVIOUS WORK ON STRUCTURED LIGHT SCANNERS

Structured light based 3D scanning systems are cost effective and practical. The main problems of line laser systems are calibration, occlusion, external lighting, and surface structure. Since laser is a powerful light source, the surface structure and lighting conditions affect the scanning result. Also positioning, control of the light source, and the camera orientation create calibration and occlusion problems. Davis and Chen [1] worked on reducing the calibration complexity of the range information using two cameras. They used the second camera for controlling the calibration of range information. As a result, they acquired the same accuracy of calibration with less cost and complexity. Stocher and Biegelbauer [2] used a different calibration technique for laser scanners. They used a wire frame model. The edges of the model are made of aluminum profiles. This makes point correspondences more robust without a need of intensity information. Furthermore this structure allows multi-view calibration.

Godin *et al.* [3] worked on calibration of range camera. They proposed active triangulation. In this method, by the help of a mirror the stripe is projected to a series of positions. The positions of the stripe is detected by a linear position detector. These positions are compared with bar at a known position. By applying a general equation derived for triangulation, they produced guidelines. These guidelines help the preliminary design of the camera.

Fasano *et al.* [4] worked on the occlusion problem in 3D range scanning. Occlusion mostly occurs in indented surfaces. The laser stripe cannot reach some parts of the surface. Another reason for occlusion is that the camera angle restricts capturing some areas of the object. Fasano *et al.* proposed to use mirrors on laser scanners to allow the scanning of hard-to-reach parts. By a rotary table and by two flat mirrors, the laser line reaches the inner parts of the object. Marc *et al.* [5] used two cameras to solve the occlusion problem. They also proposed a method for combining two images into a single range image. They applied translation and rotation methods to the two images according to the angle of view to combine them. Hyun and Gerhardt [6] investigated errors on the triangulation process on laser scanners and showed the effects of occlusion. They compared the effects of perspective

view. They showed that, this causes large errors on absolute and relative depth estimation. They also showed that scanning with one line increases the triangulation error.

Franca *et al.* [7] proposed to scan objects on two axes and change the field of view to increase the accuracy on range. The object is scanned both on horizontal and vertical axis. By a reconstruction algorithm, they fused the two scan data. At the end, they obtained a more accurate range information using this strategy.

Chung and Liao [8] proposed a system for scanning general objects like toys or daily life objects. They proposed using more than one laser with different intensities. They aimed at reducing the effect of light intensity. This is mainly the glaring of laser light on the surface on the captured image. The system projects each laser to the object and decides the best intensity value. Therefore, they make a laser power optimization to obtain the best result from the surface reflection.

Tsakiri and Ioannidis [9] mentioned the problems on reflection and lighting conditions while scanning the ancient statue of Hermes by Praxiteles. Because of the marble structure of the statue, the laser is scattered and reflected during scanning. Therefore, they obtained a noisy scan data. They also provided the scanning comparison between the opaque plaster and the marble parts of the statue. The noise level obtained while scanning the plaster parts are much more lower than the marble parts. To solve these type of surface problems, Forest *et al.* [10] proposed an FIR filter approach. They aimed to locate the laser on different types of surfaces. Therefore, they designed a filter structure according to the surfaces with different optical properties. At the end, the stripe information is emphasized by processing the image with digital filtering techniques. Clark *et al.* [11, 12] used polarization filters to solve the problem of spurious inter reflections caused by cavities and holes on the shiny surfaced objects. Their method is based on polarizing the outgoing laser light. After reflection, the polarization of the light also changes. Therefore, by filtering the incoming light based on its polarization, they reduced the undesired reflections.

Boehler and Marbs [13] performed tests on different brand laser scanners. They compared the scanners on different surfaces and different edge structures. Laser scanners are

known to produce noise on sharp edges. They compared the accuracy and level of noise of these scanners. Their results showed that aluminium foil type rough surfaces with high reflectance has the worst condition on scan results. Also scanners had the highest accuracy on white and gray colored objects. Petrov *et al.* [14] also performed a comparison of commercial scanners. They showed the limitations of the laser scanners because of the hardware incapabilities. They concluded that, the improvement on the camera sensor technology will also improve the scanner resolution and accuracy.

One of the most important 3D scanning applications is the "The Digital Michelangelo Project". This project aims to 3D scanning of large statues of Michelangelo. The scattering of the laser on the marble is explained in detail in this study. Marble is composed of densely packed crystals. The laser that hits the crystal scatters. This causes a view of spot as shown in Fig. 2.1.

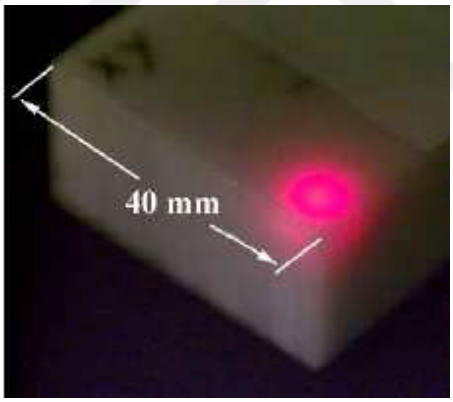

Figure 2.1. Photograph of a focused 633-nanometer laser beam 120 microns in diameter striking an unpolished sample of Carrara Statuario marble. (Photo courtesy of National Research Council of Canada.)

This scattering creates the problem of localization of the laser. Most of the scanners localize the stripe according to its center. Since the stripe is scattered like a spot, it is not possible to find the right location of the center. As shown in Fig. 2.2 the bias of the scattering depends on the angle of view and the angle of incidence [15].

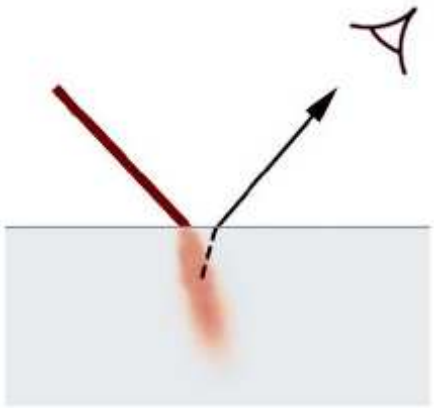

Figure 2.2. The scattered light forms a volume below the marble surface, leading to noise and a systematic bias in derived depth.

Levoy *et al.* [15, 16] designed their own laser scanner for this project. The David statue as shown in Fig. 2.3 is one of the famous application of this project.

The scanner is placed closed to the object to have a high resolution range data. Levoy *et al.* tried different lighting conditions, to decrease the effect of laser scattering. They scanned the same surface more than once with high and low illumination. They chose the best result for each part of the scanning. Then, they combined these parts to get the 3D scan of the statue.

Godin *et al.* [17] also studied the 3D scanning of archeological findings. They also mentioned the laser scattering problem occurring on the marble. They designed their own type of sensors to overcome this problem. They made experiments on archeological objects. Their sensor gave accurate results on most of their test set. However, they also had a problem on scanning marble as Levoy *et al.* did.

Guidi *et al.* [18] also mentioned the same problem, in their archeological scanning project. They worked on the project on digitizing Donatello's "Maddalena", which is a marble sculpture. Therefore, it had the same problems as with the David statue.

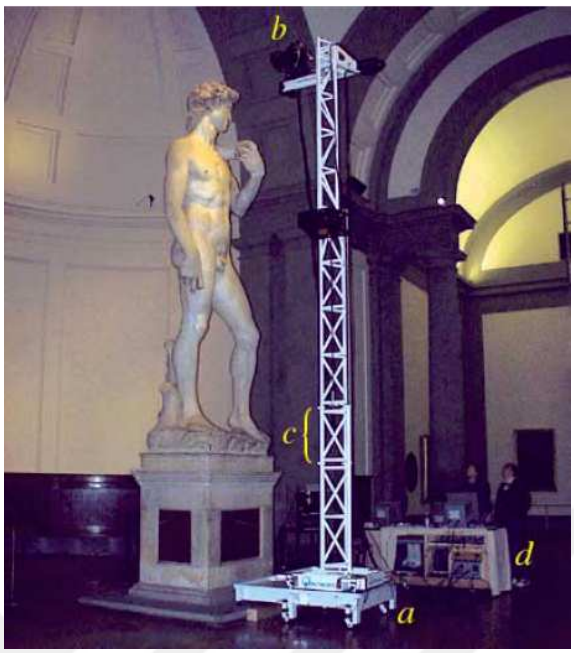

Figure 2.3. The laser scanner of Levoy in front of the David statue

Othani and Baba [19, 20] proposed a range finding approach for specular objects. They limited the angle of the light stripe that enters the lens with shield masks. This slows down the scanning speed. So, they made changes on the sensor. Their new sensor can acquire the angle of incidence directly. By this approach, they had the same accuracy with the non-specular objects.

Salvi *et al* [21], Pages *et al* [22], and Batlle *et al* [23] provided a detailed literature survey on structured light scanners. They investigated the methodologies applied for surface types, calibration complexities and the success of the described systems in the literature. They showed that, for the surface structure problems, mostly filtering is proposed. Some of these methods worked well under specific constraints. For the calibration and line extraction complexities, they showed that most of the studies focus on changing the stripe structure.

An example of scanning large areas in cultural heritage is by Kadobayashi *et al.* [24]. They made a comparison of laser scanning and photogrammetry for recording of cultural heritage. They worked on Byzantine ruins on Gemiler island at southwest of Turkey. Their

laser scanner range is 2 to 60 meters. The accuracy of the scanner is 8 mm. They also extracted 3D range from photographs. They concluded that, using both systems together is the best solution. Also, by the help of photogrammetry they can apply high level of texturing.

Blais *et al.* [25] worked on obtaining the range information of moving objects by a laser scanner. Laser scanners are hard to implement for scanning moving object. For an accurate triangulation, the laser scanner and the object should be totaly stable. They primarily get a rough and distorted data of the moving object. Then, they optimize the model by estimating the object motion. Another similar application is the robot system developed by Lin *et al.* [26]. They used a laser structured light system to find the range of obstacles in front of a mobile robot. There is a camera on the top of the robot. A horizontal laser line is projected from the front part of the robot. By processing the deformation of the laser line, the shape and the range of obstacles are obtained in real time.

Demeyere *et al.* [27] used laser scanners for telemetry. They used the laser scanner to measure the size of cylindrical objects. They can calculate the radius of such objects by applying three tangents method. Their method provides an ability to measure pipeline type structures easily.

Zagorchev and Gosthasby [28] introduced a hand held scanner. In this scanner, both the camera and the laser source have freedom of movement. The objects are placed in front of two metal frames with different sizes. The image processing algorithm makes the calibration and stripe localization according to these frames. The size and the distance of these two frames defines the accuracy of the system. this leads to a self calibrating accurate hand scanner.

Bernardini and Rushmeier [29] investigated the 3D model acquisition pipeline. They emphasized that the research should focus on the improvement of scanner systems. They mentioned the lack of automation in the 3D model acquisition. For high accuracy, there is need of man made arrangement and calibration. They also mentioned that, there is a strong need of robust data acquisition for challenging surfaces (like the ones having high reflectance). Their final comment was on the realtime feedback of the acquired surface.

3. COLOR INVARIANTS

Color invariants help extracting color properties of objects without being affected by imaging conditions. Imaging conditions can be counted as, the illumination of the environment, surface properties of the object, the highlights or shadows on the object, and the change of the angle of view. Next, we give a brief description of the surface reflection model and show how the color invariants are defined on them. Then, we consider the proposed invariants in the literature.

3.1. The Reflection Model

We aim to obtain the image of the object surface discarding the illumination conditions on it. Therefore, we first extract the surface reflection model. We can use spectral sensitivities of the RGB sensors as $f_R(\lambda)$, $f_G(\lambda)$, $f_B(\lambda)$ respectively. Gevers and Smeulders [30] represent the reflection model as

$$C = m_b(\vec{n}, \vec{s}) \int_\lambda f_C(\lambda) e(\lambda) c_b(\lambda) d\lambda + m_s(\vec{n}, \vec{s}, \vec{v}) \int_\lambda f_C(\lambda) e(\lambda) c_s(\lambda) d\lambda \qquad (3.1)$$

where $c_b(\lambda)$ and $c_s(\lambda)$ are surface albedo and Fresnel reflectance respectively. λ is the wavelength and $\vec{n}$ is the surface patch normal. The surface patch illuminated by incident light is denoted by $e(\lambda)$. $\vec{s}$ is the direction of the illumination source and $\vec{v}$ is the direction of the viewer. m_b and m_s stands for geometric dependencies of the body and surface reflection component respectively.

Assuming the white illumination conditions (equal energy density for all wavelengths within the visible spectrum), $c_S(\lambda)$ has a constant value independent of the wavelength c_S and also $e(\lambda)$ being constant e. We can define constants depending on surface albedo and the sensor as k_C. If we assume white illumination conditions

$$\int_{\lambda} f_R(\lambda)d\lambda = \int_{\lambda} f_G(\lambda)d\lambda = \int_{\lambda} f_B(\lambda)d\lambda = f \tag{3.2}$$

Then, Eqn. 3.1 becomes

$$C_W = em_b(\vec{n}, \vec{s})k_C + em_s(\vec{n}, \vec{s}, \vec{v})c_s f \tag{3.3}$$

Gevers and Smeulders consider Eqn. 3.4 as body reflection model and represent it with a body reflection vector $\vec{B}$ in the RGB color space. They also consider Eqn. 3.5 as surface reflection model and represent it by a surface vector $\vec{S}$ in the RGB color space.

$$C_b = em_b(\vec{n}, \vec{s})k_C \tag{3.4}$$

$$C_S = em_s(\vec{n}, \vec{s}, \vec{v})c_s f \tag{3.5}$$

Since the two components of reflection C_S and C_b are added for a given point on a surface, the observed colors must be inside the triangular plane created by the two reflection components. Gevers and Smeulders assert that any expression defining colors on this triangular plane is a color invariant for the dichromatic reflection model under a white illumination.

3.2. Illumination Independence

In this study, we aim to solve the problem of scanning shiny surfaces in daylight. By using an illumination independent color invariant, our scanning system becomes insensitive to the environment lighting and specularity of the object surface. To show the independency, we should model the image captured by the sensor. The image formation captured by a sensor for a specific wavelength λ is modeled as

$$\rho_k = \int S(\lambda)E(\lambda)R(\lambda)d(\lambda) \tag{3.6}$$

where $S(\lambda)$ corresponds to the surface reflection and $E(\lambda)$ corresponds to the illumination. $R(\lambda)$ is the response of the sensor.

Funt and Finlayson [31] showed that taking the ratio of the two color response of the sensor cancels out the effect of the illumination. This is not true for all sensor structures. It only holds for sensors having narrow band sensitivities. If the pixel location does not change and if there is no sudden change in the illumination then this model is also acceptable for all sensors. This assumption yields to the result as

$$\frac{\int S_1(\lambda)E(\lambda)R(\lambda)d(\lambda)}{\int S_2(\lambda)E(\lambda)R(\lambda)d(\lambda)} = \frac{\int S_1(\lambda)R(\lambda)d(\lambda)}{\int S_2(\lambda)R(\lambda)d(\lambda)} \tag{3.7}$$

For any location x on the surface with incident illumination e_k^x and albedo r_k^x we have a sensor response of Eqn. 3.8. By the result obtained in Eqn. 3.7, we can show that the values in Eqn. 3.9 are illumination invariant. Hence, the ratio of the two sensor responses is directly related to the ratio of the surface albedo as

$$\rho_k^x = e_k^x r_k^x \tag{3.8}$$

$$\frac{\rho_k^1}{\rho_k^2} = \frac{e_k r_k^1}{e_k r_k^2} = \frac{r_k^1}{r_k^2} \tag{3.9}$$

3.3. Hue as a Color Invariant

The characteristics generally used to separate one color from another are brightness, hue, and saturation [32]. Brightness embodies the chromatic notion of the intensity. Hue is an attribute associated with a dominant wavelength in a mixture of light waves. Hue represents the dominant color as perceived by an observer. Therefore when we call an object with its color like orange or yellow, we are specifying its hue. Hue is formulated as

$$H = \arctan(\frac{\sqrt{3}(G-B)}{(R-G)+(R-B)}) \tag{3.10}$$

where R, G and B correspond to red, green, and blue color bands of the image.

3.4. Normalized Color as an Invariant

Image normalization in general image processing applications proceeds in two stages. First the physical image formation and the dependency of the image due to given physical variable is made explicit. We define the image formation in section 3.2. Second, removing of this dependency is considered. To remove the image dependency on illumination, one of the methods that is used in practice is normalization as

$$\{\frac{R}{R+G+B}, \frac{G}{R+G+B}, \frac{B}{R+G+B}\} \tag{3.11}$$

By taking the ratio of the each color band to the sum of the all bands, we set the maximum illumination of that band be equal to the total illumination. This provides an illumination invariancy. These equations are extensively used in image processing and computer vision literature [32].

3.5. Color Invariants Proposed by Gevers and Smeulders

One of the popular applications that the color invariants are used is the image retrieval. Gevers and Smeulders [33, 30] proposed several color invariants in their image retrieval applications. We select some of their invariants for use in 3D scanners. We explain them next.

3.5.1. Color Invariants for Matte Objects

By modeling the reflectance of matte objects, Gevers and Smeulders produced several invariants for different type of objects with different types of surface structure. These invariants are grouped as first, second, and third order. They are provided in Eqns. 3.12, 3.13, and 3.14 respectively as

$$\{\frac{R+G}{B}, \frac{3G+B}{R+B}, \frac{R+G+B}{G+B}, \frac{4R+G}{R+G+B}, \frac{R}{R+G+B}, ...\} \tag{3.12}$$

$$\{\frac{R^2+BG}{B^2}, \frac{3GR+GB}{R^2+B^2}, \frac{R^2+G^2+B^2}{G^2+B^2}, \frac{4RG+GB}{GR+BG+B^2}, \frac{R^2}{R^2+G^2+B^2}, ...\} \tag{3.13}$$

$$\{\frac{R^3+RBG}{RB^2}, \frac{3GR^2+GB^2}{R^3+B^3}, \frac{R^3+G^3+B^3}{G^3+B^3}, \frac{4R^2G+GB^2}{GR^2+BG^2+B^3}, \frac{R^3}{R^3+G^3+B^3}, ...\} \tag{3.14}$$

Among these, we use the following ones as color invariants in this study.

$$\beta_1 = \frac{R}{R+G+B} \tag{3.15}$$

where β_1 is also the normalized red color.

$$\beta_2 = \frac{R^2}{R^2+G^2+B^2} \tag{3.16}$$

$$\beta_3 = \frac{R^3}{R^3+G^3+B^3} \tag{3.17}$$

Gevers and Smeulders proposed a new set of color invariants for matte objects as

$$c_1 = \arctan \frac{R}{max\{G, B\}} \tag{3.18}$$

$$c_2 = \arctan \frac{G}{max\{R, B\}} \tag{3.19}$$

$$c_3 = \arctan \frac{B}{max\{R, G\}} \tag{3.20}$$

The c_1, c_2, c_3 space basically extracts a feature of each band by taking the ratio of it to the maximum of the other two.

3.5.2. Color Invariants for Shiny Objects

For the shiny objects Gevers and Smeulders produced several color invariants. Also these invariants are independent of illumination intensity and direction. Similar to the previous section, these invariants are grouped as first, second, and third order. They are provided in Eqns. 3.21, 3.22, and 3.23 respectively as

$$\{\frac{(R-G)}{(R-B)}, \frac{(B-G)}{(R-B)}, \frac{(R-G)+(B-G)}{(R-B)}, \frac{(R-G)+3(B-G)}{(R-B)+2(R-G)}, ...\} \tag{3.21}$$

$$\{\frac{(R-G)(R-B)}{(R-B)^2}, \frac{(B-G)(R-B)}{(R-B)^2}, \frac{(R-G)^2+(B-G)^2}{(R-B)^2}, \frac{(R-G)^2+3(B-G)^2}{(R-B)^2+2(R-G)^2}, ...\} \tag{3.22}$$

$$\{\frac{(R-G)^3}{(R-B)^3}, \frac{(B-G)^3}{(R-B)^3}, \frac{(R-G)^3+(B-G)^3}{(R-B)^3}, \frac{(R-G)(R-B)(G-B)+3(B-G)^3}{(R-B)^3+2(R-G)^3}, ...\} \tag{3.23}$$

Among these, we use the following in this study.

$$\gamma_1 = \frac{(R-G)^2+3(B-G)^2}{(R-B)^2+2(R-G)^2} \tag{3.24}$$

Gevers and Smeulders also proposed the l_3 color invariant for shiny objects as color invariants. This space extracts a feature from the ratio of the squared differences of the color bands. The invariants are as

$$l_3 = \frac{(G-B)^2}{(R-G)^2+(R-B)^2+(G-B)^2} \tag{3.25}$$

4. NORMALIZED COLOR INDEX AS AN INVARIANT

The color invariant used in this project is originated from a previous study on multi-spectral satellite images [34]. There, a PCA transformation matrix is applied to the data in order to decorrelate the color components. By projecting the components to the uncorrelated random variables and calculating their slope, the normalized difference vegetation index is obtained. Here, we apply the same procedure to RGB images to obtain a new color invariant.

4.1. Principal Component Analysis (PCA)

PCA is a methodology for linearly transforming a correlated data set into a new space which has uncorrelated components [35]. The correlated data set is rotated about the origin to obtain the new space. For a set of correlated random vectors $\mathbf{X}$ the linear transformation matrix $\mathbf{A}$ is calculated. $\mathbf{X}$ is a $d \times n$ matrix. d is the dimensionality of the measurement, that is two for our case (we use two color bands as red and green). n is the number of data vectors, which corresponds to the number of observations.

$$\mathbf{X} = (\mathbf{x}_1, \mathbf{x}_2, ..., \mathbf{x}_n) \tag{4.1}$$

To calculate the transformation matrix, first we obtain the covariance matrix as

$$C_x = E[(X - \mu_x)(X - \mu_x)^T] \tag{4.2}$$

where μ_x is the mean of the sample vector. Next, eigenvectors a_i that satisfy Eqn. 4.3 is calculated

$$\mathbf{C}_x\mathbf{a}_i = \lambda_i\mathbf{a}_i \;\; i = 1, 2, ..., d \tag{4.3}$$

The eigenvalue-eigenvector pairs are indexed such that $\lambda_1 \geq \lambda_2 \geq ... \geq \lambda_d$. We also normalize the eigenvectors as $||\mathbf{a}_i|| = 1 \; \forall \; i$. The value of λ_i corresponds to the mean-square excursion of the data (with respect to its mean) along the direction of $\mathbf{a}_i$. The transformation matrix $\mathbf{A}$ is then formed by stacking the eigenvectors, one per row as

$$A = \begin{bmatrix} \mathbf{a}_1^T \\ \mathbf{a}_2^T \\ . \\ . \\ . \\ \mathbf{a}_n^T \end{bmatrix} \tag{4.4}$$

When this transformation is applied to any data vector x_j, it is projected onto each eigenvector as

$$\mathbf{p}_j = \mathbf{A}\left(\mathbf{x}_j - \mu_{\mathbf{x}}\right) \tag{4.5}$$

For our derivations, we shift the principal components by transformed means as

$$\mathbf{pc}_j = \mathbf{A}\mathbf{x}_j \tag{4.6}$$

where $\mathbf{pc}_j = \mathbf{p}_j + \mathbf{A}\mu_{\mathbf{x}}$; we therefore work in non-centered spaces.

4.2. Defining a New Color Invariant

To define the new color invariant, we transform the color components to an uncorrelated space. The primary stage of our color invariant definition is estimating the transformation matrix $\mathbf{A}$. The eigenvectors inside $\mathbf{A}$ are based on the samples obtained. Then, the color components are projected to the uncorrelated variables by $\mathbf{A}$. By taking normalized slope of the variables we obtain a new color invariant.

$$A = \begin{bmatrix} -\alpha_1 & \alpha_2 \\ \alpha_2 & \alpha_1 \end{bmatrix} \tag{4.7}$$

The eigenvectors $\mathbf{a}_1$ and $\mathbf{a}_2$ define the orthogonal scatter directions for the color data. By representing the color data with eigenvectors, the components are statistically decorrelated. The uncorrelated random variables pc_1 and pc_2 projected on a_1 and a_2 by

$$\begin{bmatrix} pc_1 \\ pc_2 \end{bmatrix} = A \times \begin{bmatrix} R \\ G \end{bmatrix} \tag{4.8}$$

This yields to

$$pc_1 = -\alpha_1 R + \alpha_2 G \tag{4.9}$$

$$pc_2 = \alpha_2 R + \alpha_1 G \tag{4.10}$$

The α_1 and α_2 are the correction coefficients of the color data which is related to the brightness of the image. As known, pc_1 and pc_2 are statistically uncorrelated, a slope on them can be defined as

$$\rho = \frac{pc_1}{pc_2} = -\frac{\alpha_1 R - \alpha_2 G}{\alpha_2 R + \alpha_1 G} \tag{4.11}$$

The slope defined here corresponds to the difference index of an image. We take negation to emphasize the red band in extracting color information in the following sections. An angle is defined to the corresponding slope by

$$\phi = \arctan(\rho) \tag{4.12}$$

The angle is normalized by $4/\pi$ to measure the color density. As a result, the color invariant proposed in this study is obtained as

$$\Psi = \frac{4}{\pi} \arctan\left(\frac{\alpha_1 R - \alpha_2 G}{\alpha_2 R + \alpha_1 G}\right) \tag{4.13}$$

Since we propose this invariant for the scanning shiny surfaces without effects of illumination, we should make the proof of the illumination independency of it. As we mention in section 3.2, the ratio of the sensor response is independent of illumination. If we substitute the sensor response Eqn. 3.8 to Eqn. 4.13, we have the invariant on any location x as

$$\Psi = \frac{4}{\pi} \arctan\left(\frac{\alpha_1 \rho_r^x - \alpha_2 \rho_g^x}{\alpha_2 \rho_r^x + \alpha_1 \rho_g^x}\right) = \frac{4}{\pi} \arctan\left(\frac{\alpha_1 e_r r_r^x - \alpha_2 e_g r_g^x}{\alpha_2 e_r r_r^x + \alpha_1 e_g r_g^x}\right) \tag{4.14}$$

Since we assume the illumination is white colored, the illumination coefficient e yields to single value

$$e = e_r = e_g \tag{4.15}$$

When we extract the illumination coefficient e from the parentheses, it cancels out. Therefore, we can say that Ψ is illumination invariant on white colored illumination conditions. The result of the invariant is directly related the surface albedo of the sensor response as

$$\Psi = \frac{4}{\pi} \arctan\left(\frac{e(\alpha_1 r_r^x - \alpha_2 r_g^x)}{e(\alpha_2 r_r^x + \alpha_1 r_g^x)}\right) = \frac{4}{\pi} \arctan\left(\frac{\alpha_1 r_r^x - \alpha_2 r_g^x}{\alpha_2 r_r^x + \alpha_1 r_g^x}\right) \tag{4.16}$$

4.3. An Example on Calculating Ψ

We provide Ψ calculation results for two objects (matte carafe and shiny carafe) next as given in Fig. 4.1 (a) and (b). We also provide their two dimensional histograms as shown in Fig. 4.1 (e) and (f). The eigenvalues are visualized on the scatter plot in Fig. 4.1 (c) and (d). In the figures, the red lines are eigenvectors.

We calculate the transformation matrix $\mathbf{A}$ for both images. For the matte carafe, we obtain $\mathbf{A}$ as

$$A = \begin{bmatrix} -0.7346 & 0.6785 \\ 0.6785 & 0.7346 \end{bmatrix} \tag{4.17}$$

Similarly, for the shiny carafe we obtain $\mathbf{A}$ as

$$A = \begin{bmatrix} -0.7453 & 0.6667 \\ 0.6667 & 0.7453 \end{bmatrix} \tag{4.18}$$

(a) Matte Carafe

(b) Shiny Carafe

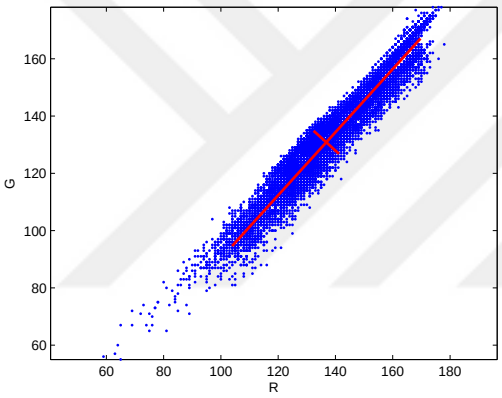

(c) Eigenvectors

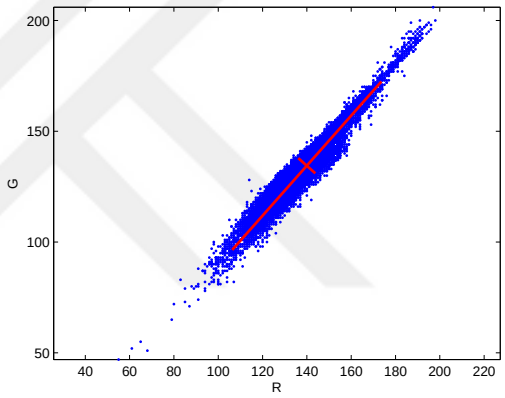

(d) Eigenvectors

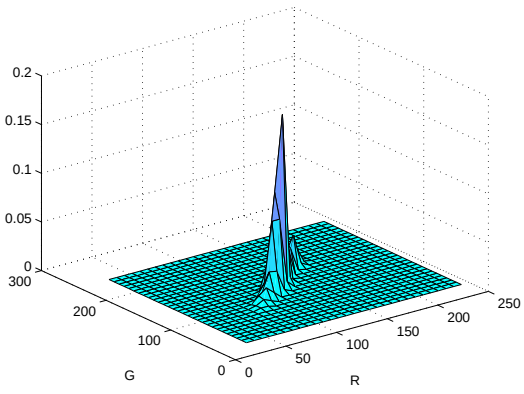

(e) Distribution

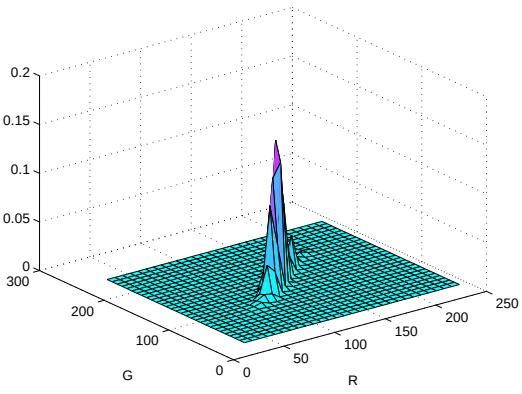

(f) Distribution

Figure 4.1. Scatter plot and eigenvectors

5. DEVELOPED RANGE SCANNERS

In this study, we have developed (both in hardware and software) two range scanners. Our first scanner is based on line laser, whereas the second one is based on a projection system. Next, we provide their design specifications in detail. In the following chapters, we will provide their advantages and disadvantages in the scanning process.

5.1. A Complete Line Laser System

Our first system is based on a line laser. The main parts of the scanner system are listed below. By the composition of these devices, a complete working system of line laser scanner is obtained. Fig. 5.1 demonstrates the working combination of these components as a block diagram. There is a line laser source placed on a stepper motor, which is driven by a micro-step driver. The control signal of micro-step driver is send by a microcontroller, which takes the rotation commands from the computer by a RS232 interface. Whole system is powered by a switch mode power supply.

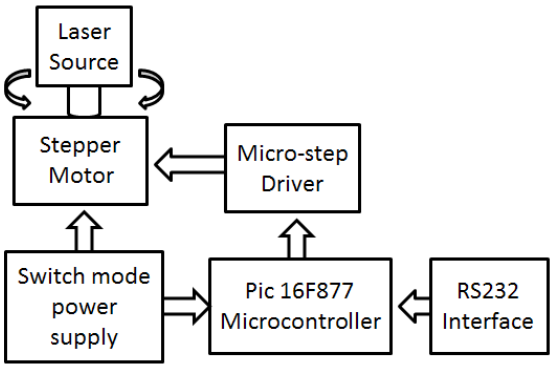

Figure 5.1. The laser scanner block diagram.

5.1.1. The Line Laser Source

The primary part of the laser system is the laser diode. Laser diode has a wavelength of $635\ nm$ which corresponds to red color in the color spectrum. In front of the diode, there is a cylindrical lens that spreads the light as a line. When the laser source is placed less than $1\ m$ away from the surface, the length of the line is $60\ cm$. The width of the line can be adjusted by adjusting the focus of the lens. In this study, we used it as $1\ mm$. The laser diode works with a $5\ V$ and $100\ mA$ power source.

5.1.2. The Step Motor and its Driver

The laser source is placed on a step motor by its special mounting. The motor works with a $24\ V$ and $2\ A$ power source. It is set to work in unipolar condition. The step motor has 1.8^o step angle. This step angle should be as small as possible to have a more accurate range scanning operation. Therefore, the step angle of the step motor is reduced by using a micro-step driver. The micro-step driver can drive any step motor working between $9\ V$ to $36\ V$ and the current values up to $3\ A$. The step size can be divided into 24 different levels using this driver. For this application, the step angle is set to 0.07^o.

The micro-step driver takes two signals as input to drive the motor. One is the input for direction and the other is the clock signal. To control micro-step driver from the computer, an interface circuit is designed. This circuit has a serial input from the computer. The serial input is taken by a PIC microcontroller and the clock output is created. According to the direction of rotation, the appropriate TTL level is provided by the microcontroller to the micro-step driver.

5.1.3. The Color Camera

The image of the laser stripe falling on the object is taken by Sony *SX-910* digital color camera. The camera has a CCD sensor and the image is processed in PAL system. The output of the camera has a Firewire interface. The image is transferred digitally to the computer by an IEEE 1394 cable. Therefore, there is no need of an extra image acquisition

card on the computer. The properties like brightness or sharpness of the image are adjusted by software. The camera does not need any external power source. It is directly supplied by the Firewire port of the computer. The lens mounting on the camera is $1/3$" C-mount. A Fujinon $5.5\ mm$ to $88\ mm$ variofocal lens is placed on this mounting. The lens can be either controlled by its motor or manually.

5.2. The Working Principle of the Laser Scanner

Next, we explain the working principle of the laser scanner developed. We will provide the details of both hardware and software specifications.

5.2.1. Hardware Setup

The basic working principle of a structured light scanner is projecting a stripe to an object. By processing the deformations of the stripe, the depth information is obtained. In our first system, the stripe source is the line laser. For the scanning process, first the object is placed on the rotary table. The table is in front of the laser source with a distance of $30\ cm$. The laser line is focused according to the object. Therefore, the stripe falling on the object has a width of approximately $1\ mm$. Also, the lens of the camera is focused according to the distance of the object. The camera is placed close to the laser source, with an 30^o looking angle to the object. This setup is formed for the triangulation process (to be explained in the following sections). This setup is shown in Fig. 5.2.

5.2.2. Image Acquisition

The first step of image processing in software is the camera initialization. The required image properties are set and sent to the camera. Also, the image acquisition port and the variable that the image will be stored is defined. Then, the first image is captured by the camera and transferred to the computer. The color bands of the image are separated in order to be used in calculating color invariants. After the application of the color invariants to the image, we have the data of laser stripe emphasized on the object.

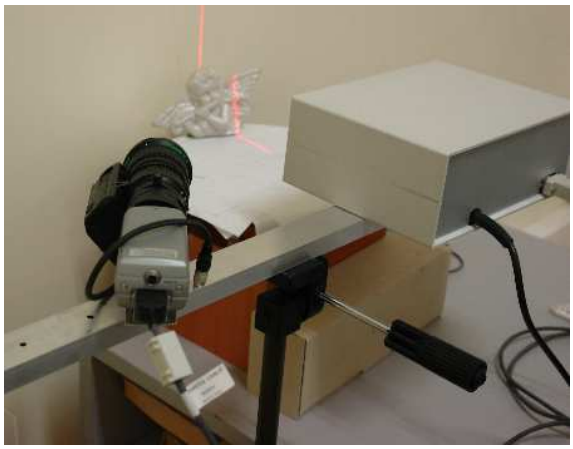

Figure 5.2. The laser scanner system developed.

5.2.3. Adaptive Thresholding

Because of different actual lighting conditions in the environment, the captured image intensity varies. In order to threshold the deformed line stripe on the object, we need an adaptive thresholding setup for the color invariant image at hand. Therefore, the histogram of the color invariant image is specified. In other saying, the sample distribution of the light intensity on the image is observed statistically. According to these statistics, the emphasized stripe data is placed over the 96% part of the histogram. Or the 96% percentile of the image is thresholded. Devore [36], defines the percentile as

$$p = F(\eta(p)) = \int_{-\infty}^{\eta(p)} f(y)dy \tag{5.1}$$

where p is the percentile. $f(y)$ is the probability distribution function. In our case, it is the actual normalized histogram of the color invariant image.

After thresholding, we applied morphological operations onto the the obtained black and white image. Gonzales and Woods [32] offer a comprehensive explanation on morpho-

logical operations. We applied opening, dilation, and erosion morphological operations to clean the image. We also applied morphological thinning to obtain a unit pixel width line to represent the line stripe.

5.2.4. Depth Acquirement

As we obtain the stripe in the image, we analyze its deformation. We need a reference point to identify the distortion of the line stripe. We assume that the upper part of the image corresponds to background. So the stripe falling on background is taken as a reference line. The stripe information falling ± 20 pixels away from this line is also accepted as background. The stripe information out of this 20 pixel tolerance is accepted as falling on the object. The distance on the horizontal axis (x) from the reference line is used to define the depth information. To extract a depth information object, camera, and the laser source is placed to form a triangle as shown in Fig. 5.3.

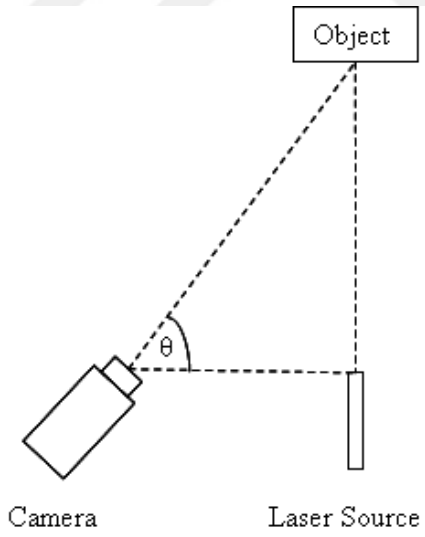

Figure 5.3. An overview of triangulation.

In this setup, the line laser source is placed perpendicular to the object. The camera makes an 60^o angle with the laser source. By using the difference on the image and the trigonometric properties of the triangle we obtain the depth information by

$$z = \frac{y_{stripe} - y_{ref}}{\cos \frac{\pi}{\theta}} \tag{5.2}$$

where z is the desired depth information. y_{stripe} is the location of stripe falling on the object in y axis. y_{ref} corresponds to the location of reference line on y axis. θ is the angle of the camera. Using the trigonometric properties of the triangle, $\cos \frac{\pi}{\theta}$ gives the depth information.

5.2.5. The Camera Calibration

In the working principle of the camera, the scene captured falls onto an image plane. On the image plane, the size of objects in real world are scaled according to the lens properties. This is shown in Fig. 5.4.

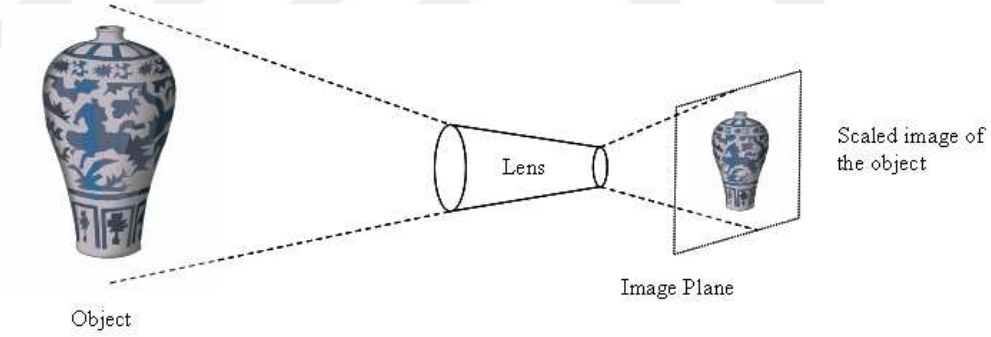

Figure 5.4. An overview of the image plane.

Therefore, the size of the object in the image we captured do not match with the actual real world size [37]. Also, the depth information obtained by Eqn. 5.2 is based on the values of the captured image. Therefore, there is a need of conversion of the image plane values to the real world values.

The Eqn. 5.3 can be used to convert the z value in Eqn. 5.2 to the real world values. Similarly, actual horizontal (X) and vertical (Y) coordinates can be found by Eqns. 5.4

and 5.5

$$Z = \frac{z \cdot f_l}{f_l + z} \tag{5.3}$$

$$X = \frac{x \cdot f_l}{f_l + z} \tag{5.4}$$

$$Y = \frac{y \cdot f_l}{f_l + z} \tag{5.5}$$

In these Eqns., f_l corresponds to the focal length of the camera. It is taken $0.007\ mm$ for our lens.

5.2.6. Feedback from The Image

As the laser scans the object, the step motor may miss some regions on the surface. This missing creates holes in the final point cloud data. To prevent this problem, the stripe location of the previous image is stored in a variable. This location is compared with the location of the new image. If there is an unexpected change on the position of the stripe, then the last movement is taken back and repeated again. This is a simple feedback control of the system. It prevents any problems occurring on the stepper motor side.

5.3. A Line Stripe based System with a Projector

We also developed a projector based system as a scanner. Here, the line stripe is generated by the projector. The working principle of this system is similar to the previously designed laser scanner. We explain their major differences next.

5.3.1. Projector Scanner Setup

A 3M LCD projector is used as the light source. It has 800×600 pixels resolution. The light stripe is formed perpendicular to the object. This system does not need any rotating or other system for moving the stripe. The stripe slides on the image projected. Here, the camera is placed with an angle of 45^o in order to get the right depth in triangulation. The whole system is placed $1.5\ m$ away from the object to decrease the affect of the powerful light source. The actual setup is given in Fig. 5.5.

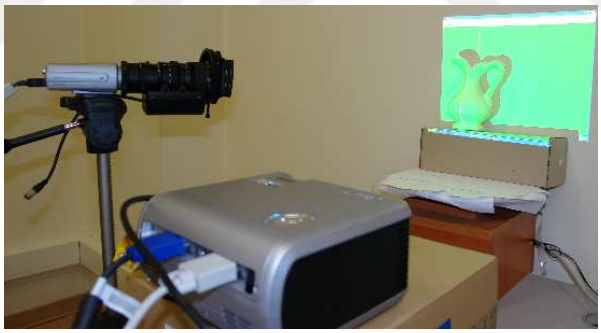

Figure 5.5. The stripe projection system implemented.

5.3.2. The Scan Process

The image processing algorithm of the projector system is completely same with the laser scanner. The difference is in the projected light stripe. In the laser system, only a laser stripe is projected. Here, the image is projected. The color invariant proposed in this project uses the information of the red and green bands. Therefore, we use the red line with a green background on the projected image. The aim here is to extract the line stripe easily. Another difference on the stripe projection system is the shadow removal part. It is explained in

detail, next.

The depth acquirement and camera calibration part of this scanner is totally the same with the laser scanner explained. The image feedback is not used here, because there is not a problem of passing over on some parts of the object. This system does not contain any moving parts and complex hardware. Therefore, the scanning process time is less than the laser scanner. On the other hand, the accuracy of the laser scanner is much more higher.

5.3.3. Removal of Shadows

The projection device is a powerful light source and the projected image covers a large area. Therefore, the shadow of the object appears on the image. Applying color invariants to shadowed images creates problems on stripe extraction. Therefore, the shadow information has to be removed before extracting the line stripe. To remove the shadow from an image, there are several methods applied by color invariants [38, 39, 40]. We use the greyscale image to remove the shadow. We converted the image captured to greyscale. Then, a threshold is applied to find the dark areas (corresponding to shadowed regions). After finding the shadowed regions, we discard it from the captured image for future processing. We provide an example for this process in Fig. 5.6. As can be seen, the shadowed regions are clearly extracted by our method.

(a) Shadow (b) Thresholded

Figure 5.6. Sitting angle, an example of shadow on stripe projection system.

6. EXPERIMENTS ON DEPTH EXTRACTION

The experiments in this study is performed in two parts. The primary part is on colors invariant that we proposed (Ψ). These experiments are made to observe the results of Ψ on different surface conditions. The second part investigates the color invariants used in the literature.

We apply these experiments on both of our range scanner systems. For the laser and stripe projecting scanner we used the same test conditions. To give a brief explanation about medium of the experiment, we have set the systems in a $50\ m^2$ room. The room is illuminated with eight fluorescent lamps. During the scan process, the room is fully illuminated. The windows of the room are covered with curtains. This is made in order to prevent the system from any change in illumination during the scan process. The object is placed on a rotating table. The background of the object is a cream colored painted wall. The paint of the wall is matte, therefore there is no effect of the paint on the experiments.

We placed the laser scanner approximately $30\ cm$ far away of the object. The laser is placed perpendicular to the object. The camera is placed with a 30^o angle to provide to the triangulation regulations. The diaphragm value of the camera lens is set to nine during the experiments. The zoom level is regulated according to the object size from $5.5\ mm$ to $20\ mm$. For a reliable comparison, we use both shiny and matte versions of the matte and shiny carafe object. This object is made of clay. The raw surface has a low specularity. Therefore, it is used for matte surface experiments. For the specular surface, we use its painted version. The paint is a glossy ceramic paint which causes the surface to be shiny.

On the stripe projection experiments, the projection device is placed $1.5\ m$ away from the object. The camera is also placed to the same distance to satisfy the triangulation conditions. The detailed explanations and experimental results are given in following sections.

6.1. Test of Ψ

On the primary part of our experiments, we apply Ψ to the image captured from the laser source. Also, we apply Ψ to the image captured from stripe projection. For experiments on shiny surfaces, we use the carafe and vase objects with glossy paint. Also, we apply Ψ to the dove that is made of porcelain material. Porcelain is also a highly specular material. To apply Ψ on matte surfaces, we choose the carafe, rectangular vase, and jar objects. They are made of raw clay. Therefore their surfaces are completely matte.

6.1.1. Test on Shiny Objects

The test objects and the results of the invariant applications is shown on the following figures. On each figure, the first image shows the object. The second is the Ψ applied and the third is the thresholded version of Ψ. For the shiny surfaces, our primary object is the carafe with glossy paint. As shown in Fig. 6.1 (a) the red colored laser hits the object. The effect of the light of the medium is also clearly seen. There is a bright area on the center of the carafe that makes the laser hard to recover. The image in Fig. 6.1 (b) shows the result when Ψ is applied. The laser stripe is clearly emphasized on the Ψ image. Also the bright area on the carafe is not seen on this image. This indicates that the invariant provides a good result on this type of shiny surface. The thresholded image matches up with this result. The line is obtained without any effect of brightness. The small points seen below the objects are caused because of the laser reflections of the surface on the rotating table.

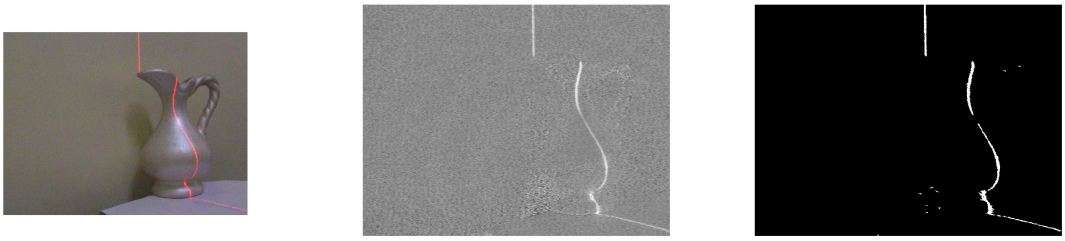

(a) Carafe with glossy paint (b) Color invariant applied (c) Threshold

Figure 6.1. Result for Ψ applied to the shiny carafe

For porcelain surfaces, the effect of shiny surface is seen on small highlights. On the

dove image in Fig. 6.2 one can see the highlights on the head and the neck of the dove. There is a small highlight on the top of its wing also. The image that shows Ψ does not contain any of these highlights. The brightest pixels of this image correspond to the laser stripe. The threshold image also proves that. The laser line is extracted without any noise. The small point reflections is also seen on this image. This again is caused because of the laser reflections from the rotating table.

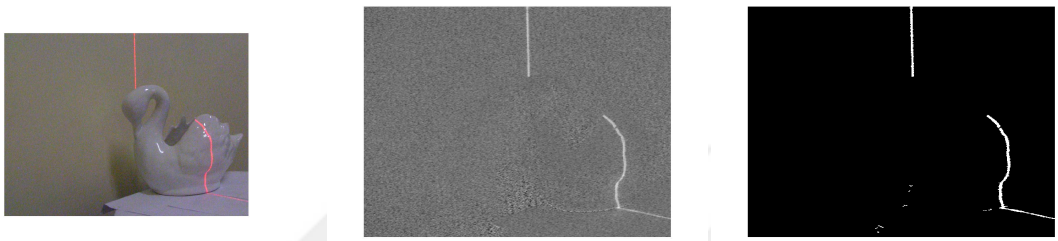

(a) Porcelain dove (b) Color invariant applied (c) Thresholded

Figure 6.2. Result of Ψ applied to porcelain dove

The experiment on the vase with glossy paint is made with stripe projection system. As seen in Fig. 6.3 (a) there is a bright area at the center of the vase. Also the shadow of the object that hits the wall is seen. The bright area is not seen on the Ψ image. It covers the laser stripe and the shadow information. The threshold image also contains the background and the laser information. It can also be seen from the threshold that stripe projection system gives a rough line which keeps from having high details.

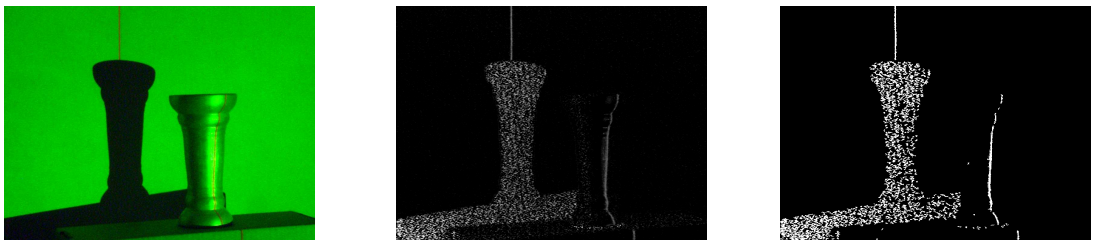

(a) Vase with glossy paint (b) Color invariant applied (c) Thresholded

Figure 6.3. Result for Ψ applied shiny vase

6.1.2. Test on Matte Objects

We make the matte experiments on carafe, rectangular vase, and jar objects. Fig. 6.4 shows the results obtained by applying Ψ to the matte carafe. Since the surface is matte, there is not any shiny or specular part on the image. On Ψ image we can see that the laser stripe has the higher pixel values. The threshold contains the clear line data. The small points of shadow also can be seen on this image.

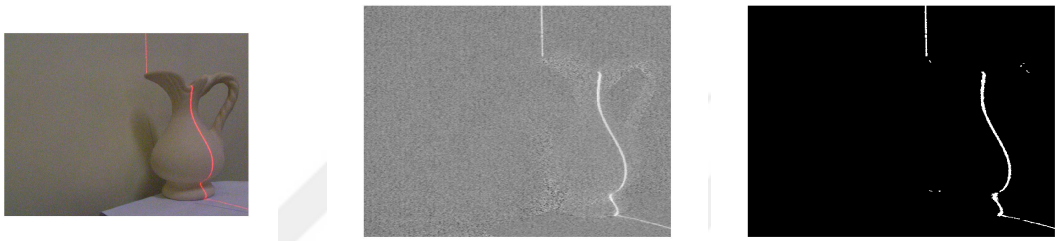

(a) Carafe without paint (b) Color invariant applied (c) Thresholded

Figure 6.4. Result for color invariant applied matte carafe

The other matte object is the rectangular vase shown in Fig 6.5. Since it as also a matte surface there is not seen any brightness on the image. The Ψ image has clearly emphasized the laser line. The threshold image is totally clean. It only contains the laser stripe. The effect of reflecting dots is not seen on this image.

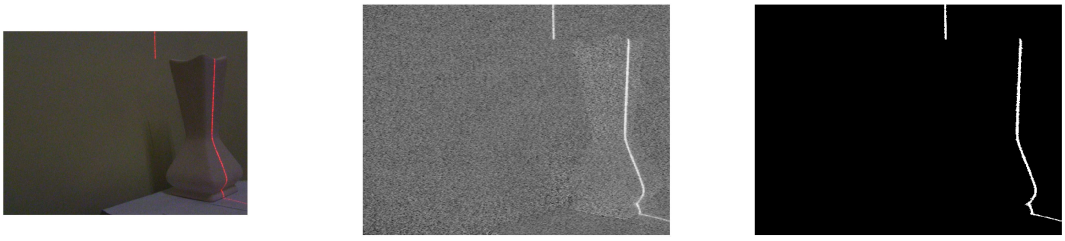

(a) Rectangular vase without paint (b) Color invariant applied (c) Thresholded

Figure 6.5. Result for Ψ applied matte rectangular vase

The test made for the stripe projecting system is shown in Fig. 6.6. The whole image has a smooth illumination. There is not any bright regions on the object. The red stripe can be seen explicitly. The Ψ image contains the points occurring from shadow and the red line on the object. The threshold image extracts these spots of shadow. But also the stripe on the

object is obtained without any loss. Also on this image, it is seen that the stripe projector gives a rough line so there is a loss in details.

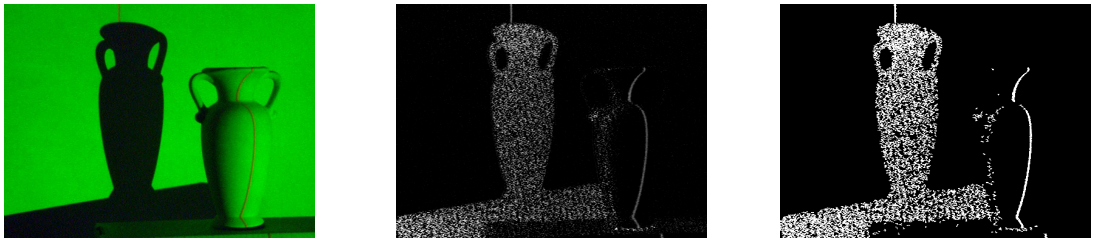

(a) Jar without paint (b) Color invariant applied (c) Thresholded

Figure 6.6. Result for Ψ applied matte jar

6.2. Comparison of Line Laser and Projection based Systems

We test our two scanners on matte and shiny carafe below. Both the laser and the stripe projection systems the matte surfaces give line information clearly. Since the surfaces are matte there is not any bright or specular points on the images captured. The Ψ image emphasizes the red color accurately on both of the systems. There for for the matte surfaces the threshold of the both of the systems give the exact lines that are projected.

For the shiny surfaces as shown in Fig 6.8 (a) and (d) there are glowing locations on the object. The glowing part on the laser system is the reflection of the light of the medium. However on the stipe projection system glowing part is the reflection of the projection light. When Ψ is applied the line is obtained clearly on both of the systems. But, in Fig. 6.8 (c) one can see a location that has a break down on the stripe. This is caused because of the highest glowing point on the surface of the carafe. In other words, the fluorescent light in the room we perform the experiment hits directly to that point. Therefore the laser illumination is lower than the medium light at that point. This causes a loss of laser data there.

The tests on Ψ showed that the shadow information is also extracted with the red color data. Laser scanner projects the stripe on to the object. So, there is not any of shadow caused by light source. Therefore the extracted data completely corresponds to the laser stripe. However stripe projection system projects light to the whole surface. Therefore it creates

an explicit shadow of the object. When Fig 6.7 (b) (e) are compared, the extraction of the shadow on stripe projection system can be seen. This causes a shadow removal process in the threshold stage. Since only the laser line is thresholded, the laser line is obtained with a smooth structure without any loss in detail. However, the threshold of stripe projecting system gives a rough stripe. This is caused because of the shadow removal process. Therefore, we can not scan objects with high details by our stripe projecting system.

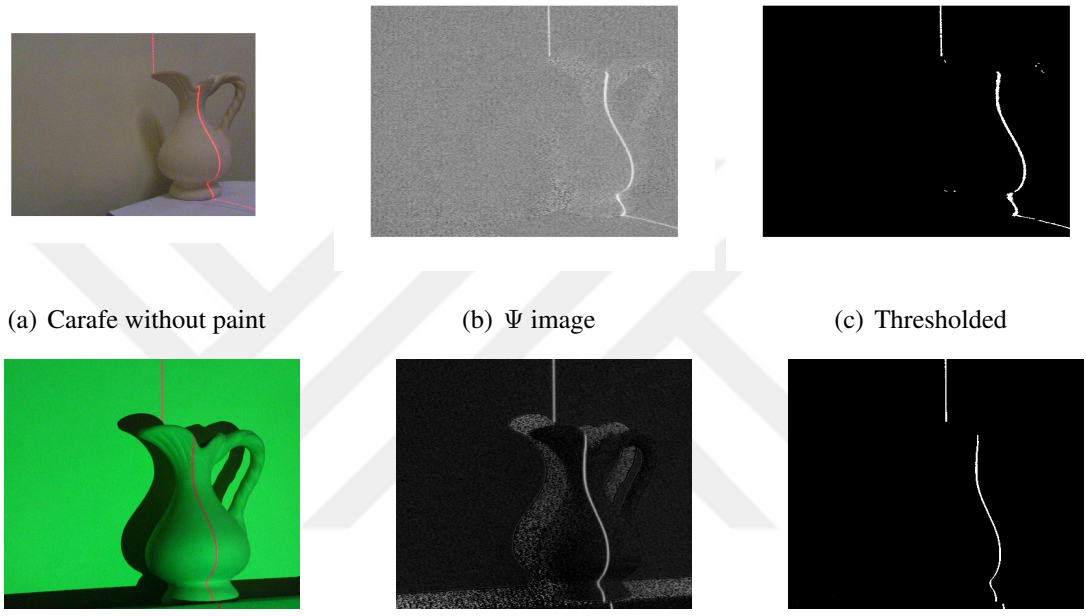

(a) Carafe without paint (b) Ψ image (c) Thresholded

(d) Carafe without paint (e) Ψ image (f) Thresholded

Figure 6.7. Comparison of line laser and projection machine on matte carafe

6.3. Comparison of Different Color Invariants

On the second part of our experiments we have applied methods that are used on color application studies. We applied each method to the carafe with paint and without paint to compare the success on shiny and matte surfaces for extracting the line data. Here we demonstrate and give the detailed explanations of the best results obtained on line extraction.

6.3.1. Extracting Data from the Red Band Image

Primary method we applied is looking to the color band to recover the line with that color. Since our system uses red colored laser we test the success of the red band line

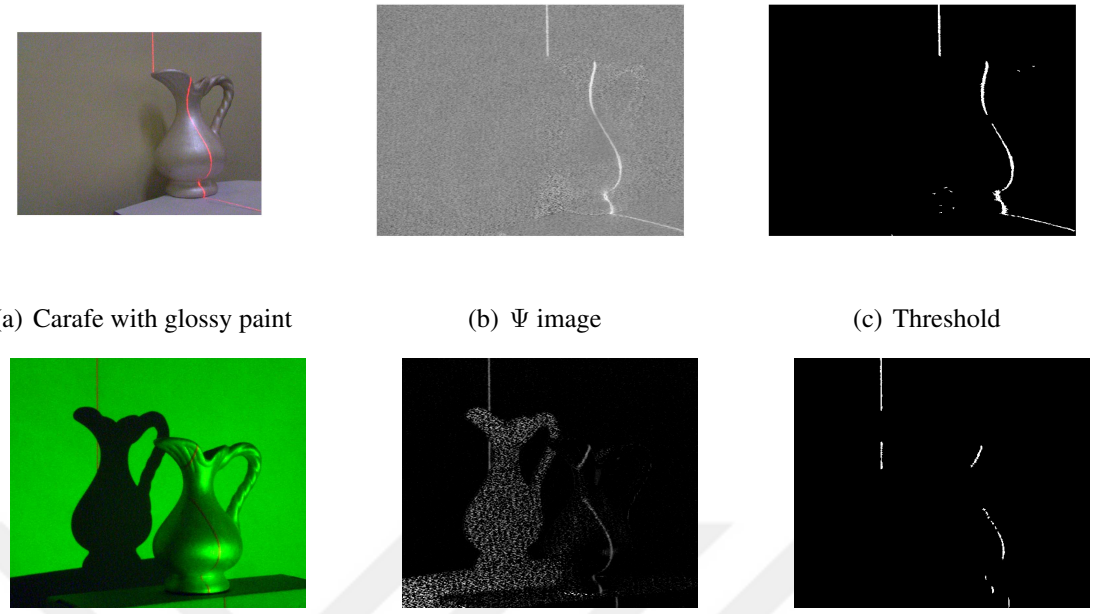

(a) Carafe with glossy paint (b) Ψ image (c) Threshold

(d) Carafe with glossy paint (e) Ψ image (f) Threshold

Figure 6.8. Comparison of line laser and projection machine on shiny carafe

extraction. The results of the red band is shown in Fig. 6.9 (c) and Fig. 6.9 (d). The red band can extract the line clearly on matte surfaces since there is no any glowing parts. However, on the shiny surface the glowing part is also has a high illumination value on the image. Therefore the threshold of this image gives the glowing part with the stripe data.

6.3.2. Extracting Data from the Greyscale Image

The secondary method applied is taking the greyscale image. By taking the grayscale image we are totally interested on the illumination values. As can be seen from Fig. 6.9 (e) and Fig. 6.9 (f), the threshold of the greyscale image on matte surface gives the line clearly. Laser line has the highest illumination value on the matte surfaced image. Therefore by applying threshold the line can be extracted easily. On the shiny surface image now the light of the medium reflected from the surface has also high illumination. Therefore, by applying threshold not only the laser line but also the shining part of the object is extracted.

6.3.3. Extracting Data from Hue Information

Hue is one of the most used methods on color applications. Therefore we have also applied Hue to our system to observe the results on line extraction. Hue gives a data with noise which is shown in Fig. 6.9 (g) and Fig. 6.9 (h). Hue also emphasize the laser line and the threshold gives the line information. But, both on shiny and matte surface it has break downs on the line. The size of the breakdown is higher on the shiny surface since the illumination of the reflected light is higher o this surface. The effect of glowing part can also be seen on the grey part at the center of the carafe.

6.3.4. Extracting Data from Gevers and Smeulders Invariants

The other invariants we applied are given in Chapter 3, proposed for special application areas like color object recognition and image retrieval. Here we give the best results for line extraction of the color invariants . One of the color invariants we applied is the c_1 invariant. This invariant extracted the line information on matte surface with a success. As shown in Fig. 6.9 (i) and Fig. 6.9 (j) the threshold of this invariant contains only the line information. However, the invariant is not so successful on shiny surfaces. The invariant extracts the glowing part of the carafe with the laser line together. The result obtained from this invariant is nearly same with the red band results.

l_3 is one of the other color invariants that we applied. The result of this invariant is shown in Fig. 6.9 (k) and Fig. 6.9 (l). This invariant was successful on matte surfaces. The invariant applied image suppresses the line information. However, by taking the inverse and applying threshold gives the line information. On the shiny surfaces the glowing part of the object is also acquired. By taking the inverse we eliminate it. But the laser information located there is also lost.

γ_1 invariant has also a similar result with the l_3 invariant as in Fig. 6.9 (m) and Fig. 6.9 (n). It also extracted the line information successfully on matte surfaces. Also on this invariant the inverse of the image is taken to extract the line. There is some noise spots on the threshold image and the quality of the line is rough. On the shiny surface this invariant also acquires

the glowing part of the carafe. By taking the inverse image it is eliminated. However, also on the threshold of this image the laser at that part is lost.

β_1 invariant is one of the invariants that nearly worked on both surfaces successfully. But, this invariant highly sensitive to the shadow of the object. As shown in Fig. 6.9 (o) and Fig. 6.9 (p), the shadow that hits on the wall is extracted on both matte and shiny surface images. This invariant also suppress the glow on the shiny surface. However, this causes break downs on the line at the threshold image. The shadow extracted also appears as spot noise on the threshold. We have also made experiments on β_2 and β_3 color invariants. they have the same result with the β_1. Therefore, they are not shown on figures.

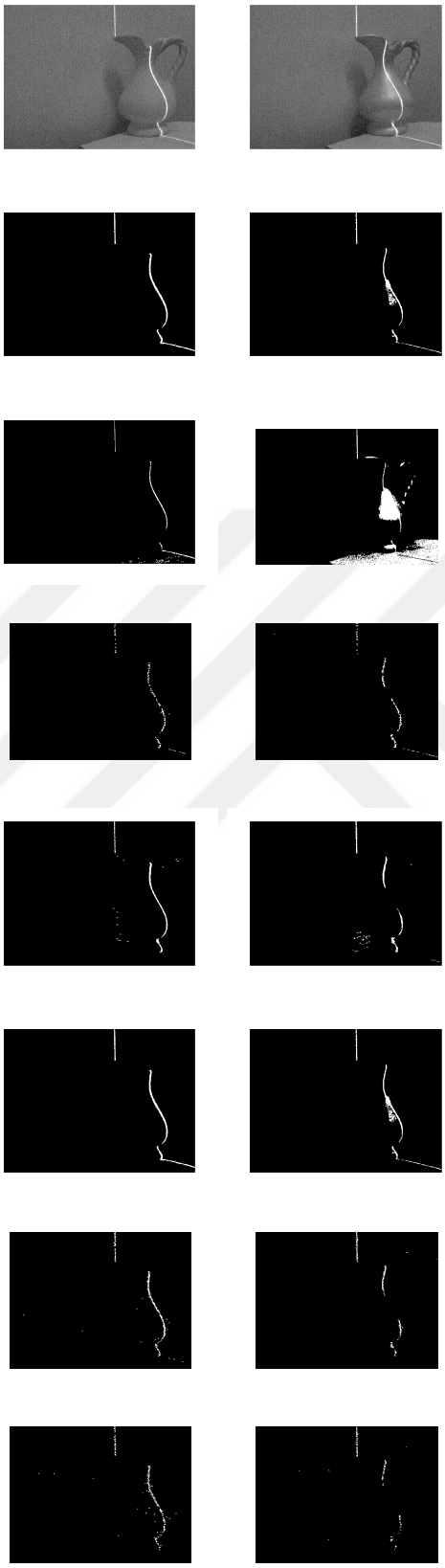

Figure 6.9. Comparison of different color invariants. The rows of the figure correspond to the Objects, red band, greyscale, hue, c_1, l_3, γ_1 and β_1 threshold results respectively. First column is the matte surface results and the second is shiny surface results.

7. FINAL RANGE IMAGES FORMED

We scanned twelve objects both with laser and stripe projecting scanners. The two of these objects have shiny porcelain surface, the seven of them has glossy painted clay surface and three objects has matte raw clay surfaces. The point cloud obtained by laser scanner is better than the stripe projecting scanner on shiny surfaces. The stripe projecting scanner has given better results on matte surfaced objects. Our interpretations about these results are based on visual observations. There is not a groundwork for a measure of comparison. In order to attain an exact measure, system should be calibrated. To have a calibrated system, the camera and the laser source should be oriented to pre measured locations with respect to the object. In practice, laser pointers are placed on the camera and the light source. These pointers project laser spots with the same orientation of the source and the camera. The spots intersect at a certain point on the object. The vertical distance of the point intersection is measured once and it is used as reference for calibration. Since, the primary purpose of this project is to give a solution to scanning shiny surfaces, we didn't make such a calibration. Therefore the comparisons range images are made on visual observations.

The point cloud obtained from the scanner is processed on the Rapidform Software. This software cleans the spot noise on the point cloud. It also removes the redundant points and make a smoothing. As a result it gives a triangular surface match of the model. On the figures given below we showed each scanned object with their point cloud and surface match obtained by laser system and stripe projecting system.

Ataturk figure is scanned with high details by the laser scanner. The Fig. 7.1 (b) shows the point cloud data of the laser scanner. The details on eye, hair and ear of the figure is clearly obtained. The point cloud shown in Fig. 7.1 (d) is the result of the stripe projecting system. This systems gives less points so the surface match of it cannot be extracted well. Also this causes the loss of details. The other detailed result is obtained by fish object shown on Fig.7.2. The laser cannot reach the back part of the fin. Therefore there is a hole occurred under the fin of the fish. Laser has also given a detailed result for the angle with flute object shown in Fig. 7.7. The hole under the arm is also the result of the occlusion of laser. From

the angle of view of the camera the laser can not be captured. The stripe projection system was not successful on extracting the model of the angel.

Column shaped vase shown in Fig. 7.3 and the vase shown in Fig. 7.12 has given clean results both on laser and stripe projection systems. Although they are shiny surfaced objects there is no effect of shine occurred on the point cloud results. As can be seen from Fig. 7.8, on the top left part of the carafe with a hole in the middle object, there is a loss of data points because of the high illumination reflecting from the surface. Similar problem occurred on the point cloud data of the shiny carafe object shown in Fig. 7.5. The center of the carafe reflects the light directly so the laser information is lost at that part of the object.

For the porcelain surfaced objects shown in Figs. 7.9 and 7.11 the system is not affected from the highlights. The point cloud results are clean. Since the projection stripe system gives less points, the surface match of the teapot object cannot be obtained successfully. The teapot result for the laser scanner contains the details of the surface articulations. The matte objects results are successful on both of the systems. In Fig. 7.4, one can see the point cloud of the jar object and the surface match of it is obtained clearly. Similarly the matte carafe shown in Fig. 7.10 and the rectangular vase in Fig. 7.6 has clear results.

(a) Ataturk

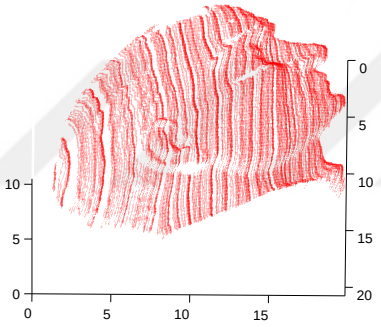

(b) Point cloud

(c) Surface

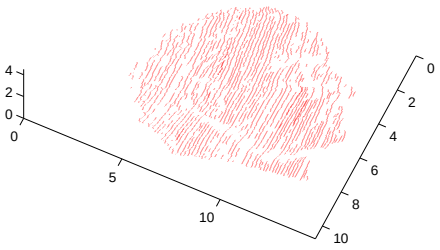

(d) Point cloud

(e) Surface

Figure 7.1. Ataturk results

(a) Fish

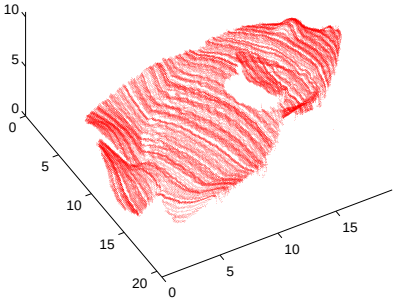

(b) Point cloud

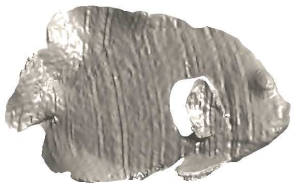

(c) Surface

Figure 7.2. Fish results

(a) Column shaped vase

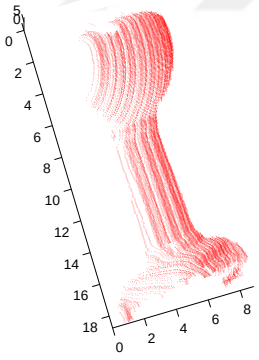

(b) Point cloud

(c) Surface

Figure 7.3. Column shaped vase results

(a) Jar

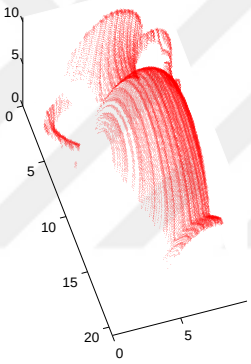

(b) Point cloud

(c) Surface

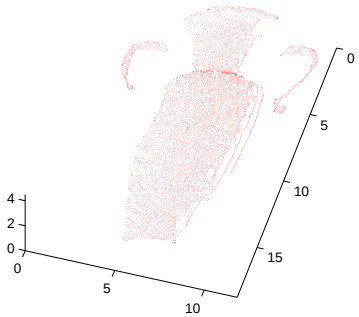

(d) Point cloud

(e) Surface

Figure 7.4. Jar results

(a) Shiny Carafe

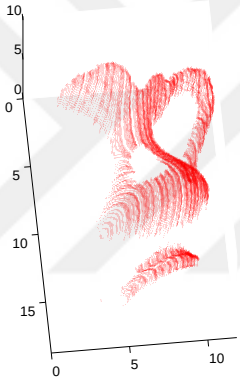

(b) Point cloud

(c) Surface

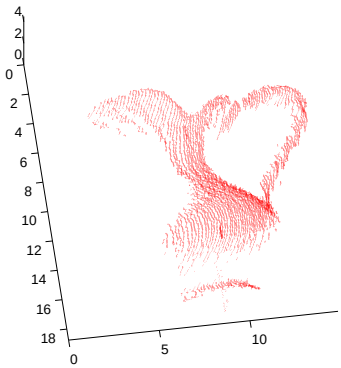

(d) Point cloud

(e) Surface

Figure 7.5. Shiny Carafe results

(a) Rectangular vase

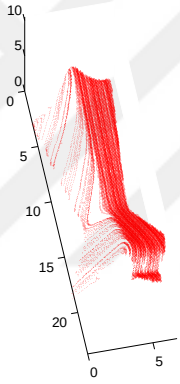

(b) Point cloud

(c) Surface

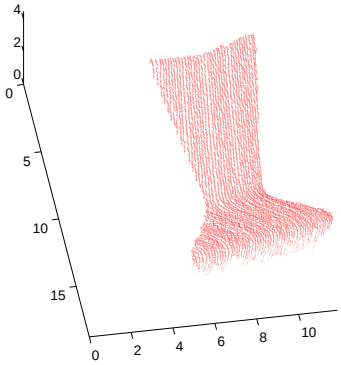

(d) Point cloud

(e) Surface

Figure 7.6. Rectangular vase results

(a) Angle with a flute

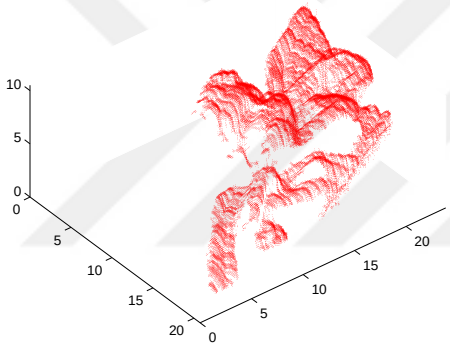

(b) Point cloud

(c) Surface

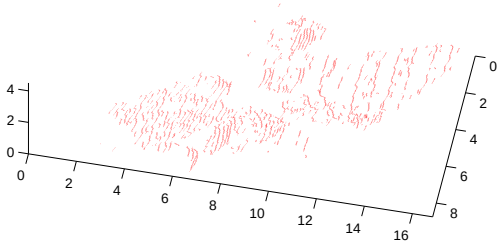

(d) Point cloud

(e) Surface

Figure 7.7. Angle with a flute results

(a) Carafe with hole in the middle

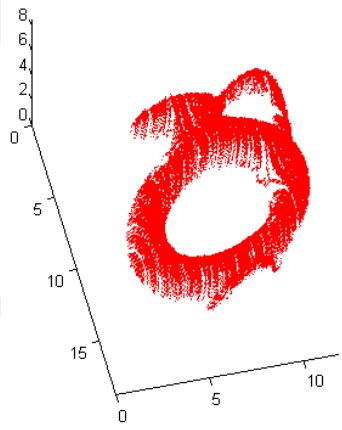

(b) Point cloud

(c) Surface

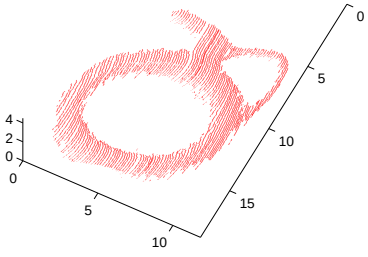

(d) Point cloud

(e) Surface

Figure 7.8. Carafe with hole in the middle

(a) Porcelain Dove

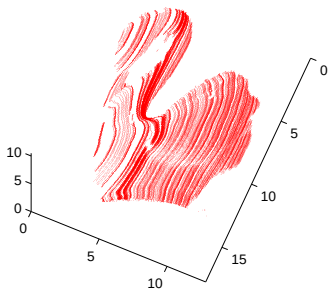

(b) Point cloud

(c) Surface

Figure 7.9. Porcelain dove results

(a) Matte Carafe

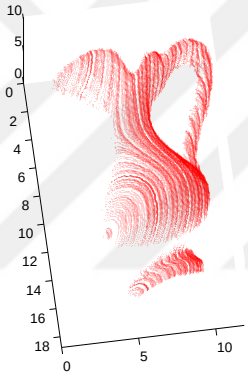

(b) Point cloud

(c) Surface

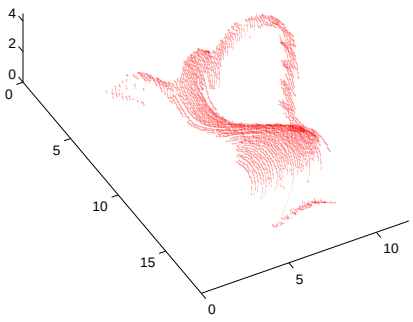

(d) Point cloud

(e) Surface

Figure 7.10. Matte Carafe results

(a) Porcelain Teapot

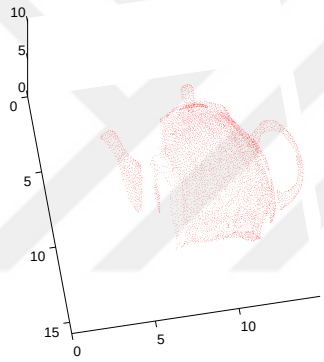

(b) Point cloud

(c) Surface

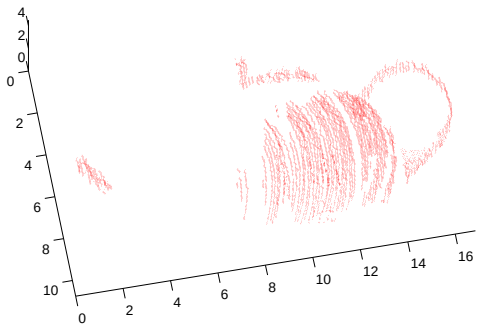

(d) Point cloud

(e) Surface

Figure 7.11. Porcelain Teapot

(a) Vase

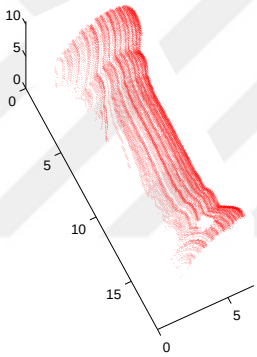

(b) Point cloud

(c) Surface

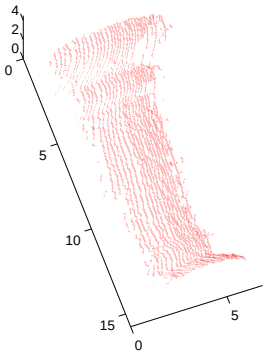

(d) Point cloud

(e) Surface

Figure 7.12. Vase

8. CONCLUSIONS

The objective of this study is to implement a 3D scanner that can scan shiny surfaces in an illuminated medium. The specularity of the surface causes problem on extracting the stripe in structured light scanners. We proposed to use color invariants to solve this problem. Color invariants help extracting color properties of objects without being affected by imaging conditions. Imaging conditions can be counted as, the illumination of the environment, surface properties of the object, the highlights or shadows on the object, and the change of the angle of view.

We proposed a new color invariant derived by principal component analysis. We also applied other color invariants that are proposed and applied in color image processing applications. A laser scanner and a stripe projecting scanner are implemented to observe the results of the color invariants. Both of the systems worked successfully for the scanning of shiny surfaces. To investigate the success of the color invariants we scanned objects with different surface structures.

Laser scanner comprise moving components like stepper motor. The stepper motor should be controlled accurately to have the laser stripe on the intended location. Therefore, there is a complex control structure that makes the laser scanner hard to implement. The resolution of the range image is related to the width of the laser line. As the line gets thinner the resolution increase. The other important parameter that affect the scanning quality is the image processing algorithm. According to the success of the image processing algorithm, the stripe information is obtained accurately to be used in depth extraction.

In our image processing algorithm we are using color invariants to have success of scanning shiny surfaces. The tests on the color invariant we proposed showed that, it can extract the stripe information o shiny surfaces accurately. We have also obtained accurate result on matte surfaces. We also applied and compared other color invariants. Our comparison showed success of some of the color invariants that are used on color image processing. As a result, color invariants worked successfully on scanning shiny surfaces on illuminated

medium.

To attain an exact measure of success there is need of calibration of the systems. Therefore, we are interpreting our results according to the visual observations. According to the observations made visually, laser scanner that we implemented has given better results than the stripe projector. The number of the data points obtained from the laser scanner is larger than the stripe projector. This causes data loss on surface match of the range image obtained by the stripe projector. The stripe projector does not contain moving parts. Therefore, it does not have a complexity of implementation. However, we can extract a rough line information. Therefore, the number of data points obtained is low.

Since the control of the stepper motor is complex, scanning an object entirely with laser scanner takes long time. Stripe projecting system is faster with respect to the laser scanner. However, both of the systems have to pass the stripe whole over the object. This makes both of the systems work slowly. They are both low cost systems in comparison with the commercial scanners. The most expensive part of the systems is the color camera.

For the heritage protection applications, using the laser scanner designed in this project will be a good choice. This type of applications do not have time limitations. Here, main requirement is not to damage the object. For instance, marble monuments placed on outdoor areas can be scanned in daylight medium without making any damage on their surface. For the art and cinema type facilities, stripe projecting system may be more useful. Because they use the scanners for face scanning type applications. Laser is a powerful light source and can give damage to eye. Therefore, using stripe projection will be safe.

REFERENCES

1. Davis, J. and Z. Chen, "*A Laser Range Scanner Designed for Minimum Calibration Complexity*", *Proceedings of the Third International Conference on 3D Digital Imaging and Modeling*, 2001.

2. Stocher, W. and G. Biegelbauer, "*Automated Simultaneous Calibration of a Multi-View Laser Stripe Profiler*", *Proceedings of the IEEE International Conference on Robotics and Automation*, 2005.

3. Godin, G., J. Beraldin and M. Riox, "*Model Based Calibration of a Range Camera*", *Proceedings, 11th IAPR International Conference on Pattern Recognition*, pp. 163–167, 1992.

4. Fasano, A., M. Callieri, P. Cignoni and R. Scopigno, "*Exploiting Mirrors for Laser Stripe 3D Scanning*", *Proceedings of the Fourth International Conference on 3-D Digital Imaging and Modeling*, 2003.

5. Marc, P., L. Jezouin and G. Medioni, "*A Versatile PC Based Range Finding System*", *IEEE Transactions on Robotics and Automation*, Vol. 7, 1991.

6. Hyun, K. and L. Gerhardt, "*The use of laser structured light for 3D surface measurement and inspection*", *Proceedings of the Fourth International Conference on Computer Integrated Manufacturing and Automation Technology*, 1994.

7. Franca, J., M. Gazziro, A. Ide and J. Saito, "*A 3D scanning system based on laser triangulation and variable field of view*", *ICIP IEEE International Conference on Image Processing*, 2005.

8. Chung, T. and C. Liao, "*An Integrated Scanning System for Reconstructing 3D Color Models of General Objects*", *Proceedings of IEEE the International Conference on Mechatronics*, 2005.

9. Tsakiri, M. and C. Ioannidis, "*Laser scanning and photogrammetry for the documentation of a large statue*", *Proceedings of Nineteenth International Symposium of CIPA*, 2003.

10. Forest, J., J. Salvi, E. Cabruja and C. Pous, "*Laser stripe peak detector for 3D scanners, A FIR filter approach*", *Proceedings of the 17th International Conference on Pattern Recognition ICPR*, 2004.

11. Clark, J., E. Trucco and H. Cheung, "*Using light polarization in laser scanning*", *Proceedings of the 6th British conference on Machine vision*, 1995.

12. Clark, J., E. Trucco and H. Cheung, "*Improving Laser Triangulation Sensors Using Polarization*", *Proceedings of Fifth International Conference on Computer Vision*, 1995.

13. Boehler, W. and A. Marbs, "*Investigating Laser Scanner Accuracy*", *XIX Symposium of CIPA*, 2003.

14. Petrov, M., A. Talapov and T. Robertson, "*Optical 3D Digitizers: Bringing Life to the Virtual World*", *IEEE Magazine Computer Graphics and Applications*, Vol. 18, pp. 28–37, 1998.

15. Levoy, M., K. Pulli and B. Curless, "*The Digital Michelangelo Project: 3D Scanning of Large Statues*", *Proceedings of SIGGRAPH*, 2000.

16. Levoy, M., P. Brunet and R. Scopigno, "*The Digital Michelangelo Project*", *EUROGRAPHICS*, 1999.

17. Godin, G., J. Beraldin and J. Taylor, "*Active Optical 3D Imaging for Heritage Applications*", *IEEE Magazine Computer Graphics and Applications*, Vol. 22, 2002.

18. Guidi, G., A. Beraldin and C. Atzeni, "*High-accuracy 3-D modeling of cultural heritage: The digitizing of Donatello's "Maddalena"*", *IEEE Transactions on Image Processing*, Vol. 13, pp. 370–380, 2004.

19. Othani, K. and M. Baba, "*A Range Finding Approach by Detecting the Position and the Incident Angle of a Light Stripe*", *IEEE Instrumentation and Measurement Technology Conference*, 2002.

20. Othani, K. and M. Baba, "*A New Laser Rangefinder for Measuring 3-D Shapes of Specular Objects in a Real Environment*", *SICE Annual Conference in Sapporo*, 2004.

21. Salvi, J., J. Pages and J. Battle, "*Pattern codification strategies in structured light systems*", *Pattern Recognition*, Vol. 37, pp. 827–849, 2004.

22. Pages, J., J. Salvi, R. Garcia and C. Matabosch, "*Overview of coded light projection techniques for automatic 3D profiling*", *Proceedings of IEEE International Conference on Robotics and Automation, ICRA*, 2003.

23. Batlle, J., E. Mouaddib and J. Salvi, "*Recent progress in coded structured light as technique to solve the correspondence problem: a survey*", *Pattern Recognition*, Vol. 31, pp. 963–982, 1998.

24. Kadobayashi, R., N. Kochi, H. Otani and R. Furukawa, "*Comparison And Evaluation Of Laser Scanning And Photogrammetry And Their Combined Use For Digital Recording Of Cultural Heritage*", *XXth ISPRS Congress*, 2004.

25. Blais, F., M. Picard and G. Godin, "*Accurate 3D acquisition of freely moving objects*", *Proceedings of the 2nd International Symposium on 3D Data Processing, Visualization, and Transmission*, 2004.

26. Lin, I., F. Wallmer and R. Dillmann, "*An Advanced Telerobotic Control System For A Mobile Robot With Multisensor Feedback*", *Proceedings of Intelligent Autonomous Systems*, 1995.

27. Demeyere, M., E. Dereine, C. Eugene and N. V., "*Measurement of Cylindrical Objects Through Laser Telemetry: Application to a New Forest Caliper*", *IEEE Transactions on Instrumentation and Measurement*, Vol. 51, 2002.

28. Zagorchev, L. and A. Goshtasby, "*A paintbrush laser range scanner*", *Computer Vision and Image Understanding*, Vol. 101, 2005.

29. Bernardini, F. and H. Rushmeier, "*The 3D Model Acquisition Pipeline*", *Computer Graphics Forum*, Vol. 21, 2002.

30. Gevers, T. and W. M. Smeulders, "*Content-Based Image Retrieval by Viewpoint-Invariant Color Indexing*", *Image and Vision Computing*, Vol. 17, pp. 475–488, 1999.

31. Funt, B. and G. Finlayson, "*Color Constant Color Indexing*", *IEEE Transactions on Pattern Analysis and Machine inteligence*, Vol. 17, 1995.

32. Gonzalez, R. C. and R. E. Woods, *Digital Image Processing*, Prentice Hall, 2 edn., 2002.

33. Gevers, T. and W. M. Smeulders, "*Combining Color and Shape Invariant Features for Image Retrieval*", *IEEE Trans. on Image Processing*, 2000.

34. Ünsalan, C. and K. L. Boyer, "*Linearized Vegetation Indices Based on a Formal Statistical Framework*", *IEEE Transactions on Geoscience and Remote Sensing*, Vol. 42, pp. 1575–1585, 2004.

35. Jollife, I., *Principal Component Analysis*, Springer, 2 edn., 2002.

36. Devore, J., *Probability And Statistics for Engineering and Sciences*, Thomson, 6 edn., 2004.

37. Trucco, E. and A. Verri, *Introductory Techniques for 3-D Computer Vision*, Prentice Hall, 1998.

38. Salvador, E., A. Cacallaro and T. Ebrahimi, "*Cast shadow segmentation using invariant color features*", *Computer Vision and Image Understanding*, Vol. 95, pp. 238–259, 2004.

39. Tsai, V. J. D., "*A comparative study on shadow compensation of color aerial images in invariant color models*", *IEEE Transactions on Geoscience and Remote Sensing*,

Vol. 44, pp. 1661–1671, 2006.

40. Yuan, X., D. Goldman, A. Moghaddamzadeh and N. Bourbakis, "*Segmentation of Colour Images with Highlights and Shadows sing Fuzzy-like Reasoning*", *Pattern Analysis and Applications*, Vol. 4, pp. 272–282, 2001.